Picture removed due to copyright restrictions.

Original available online: https://www.natureaustralia.org.au/what-we-do/our-priorities/oceans/ocean-stories/restoring-shellfish-reefs/gulf-st-vincent/

Picture Anita Nedosiko/The Nature Conservancy

Impacts of a shellfish restoration reef on wave attenuation within the Glenelg shellfish reef

By

Giorgia Bovari

Thesis
Submitted to Flinders University
for the degree of

Master of Environmental Management

College of Humanities, Arts and Social Sciences

November 2021

TABLE OF CONTENTS

ABSTRACT

Shellfish reefs have been an ecological, economic, and engineering resource since the early 1800s, with numerous species of oysters representing a key resource for fishing activities. Due to overexploitation, shellfish reefs are now considered at risk, as are the ecosystem services they guarantee. For this reason, more and more shellfish reef restoration projects are being implemented in the United States, Europe, and Australia. In South Australia there are currently four shellfish reef restoration projects, the Windara Reef in the Yorke Peninsula, the Glenelg Shellfish Reef in Adelaide, and two incomplete oyster reefs in O'Sullivan Beach and Kangaroo Island. Some of the above-mentioned countries, shellfish reef restoration projects have proved to be a sustainable and successful method, not only for the conservation of local species and their biotic and economic importance, as well as for coastal environments. However, it is important to analyse how reefs affect the hydrodynamics of the adjacent environment, in order to evaluate the performance of the structure, regarding its role on potential coastal protection. The current study developed a Delft3D numerical model to estimate the capability of the Glenelg shellfish reef in relation to potential wave energy dissipation, significant wave height reduction and attenuation of wave-driven currents. Furthermore, a two-days FLOW module testing was simulated to highlight the influence of the Glenelg reef on tidal currents and bed shear stress. The obtained results showed a minimal ability of the current reef, to influence the hydrodynamics of the area, with bigger effects during storm periods. The numerical model was subsequently validated by comparing the obtained results with wave data collected by SA Water with a pressure sensor. The validation process showed the ability of the model to pick up the wave trend, mostly during the days defined as "calm" (lower significant wave height), while it showed an overestimation of the data during the days defined as "storm" (higher significant wave height).

DECLARATION

I certify that this thesis does not incorporate without acknowledgment any material previously submitted for a degree or diploma in any university; and that to the best of my knowledge and belief it does not contain any material previously published or written by another person except where due reference is made in the text.

Signed*Giorgia Bovari*.....

Date.....3-11-2021.....

ACKNOWLEDGEMENTS

I would like to acknowledge the Kaurna people, the Boon Wurrung / Bunurong people, and the Wathaurong/Wadawurrung; I would like to pay my respects to their Elders past and present. I would like to thank from the bottom of my heart, my Supervisor, Dr. Graziela Miot da Silva for the help, support, and patience she showed me in the past few months; I could never have reached this milestone without her guidance and knowledge. I would also like to thank my Co-Supervisor, Dr. Arnold Van Rooijen for the constant support and help in understanding the Delft3D software and for making me passionate about it. I would like to thank the guys from the BEADS Laboratory at Flinders University for their valuable advice during my journey. Finally, I would like to thank my husband Andrea, my mother Sabrina, my father Gianluca and all my friends, in Italy and Australia who supported me during the months I spent studying and researching, I love you and I would not be here without you.

LIST OF FIGURES

LIST OF TABLES

INTRODUCTION

1.1 Background

In the early months of 2019, The Government of South Australia, in collaboration with the Department for Environment and Water and The Nature Conservancy announced the allocation of $ 1.2 million for a second shellfish reef restoration project in South Australia, establishing three potential areas for the new reef construction. The three proposed locations for the new shellfish reef were Glenelg, between the Glenelg jetty and the West Beach boat ramp, O'Sullivan Beach, located between Christies Beach and O'Sullivan Beach boat ramp, and Port Noarlunga, between the Port Noarlunga jetty and the beginning of the Onkaparinga River, as seen in Figure 1.

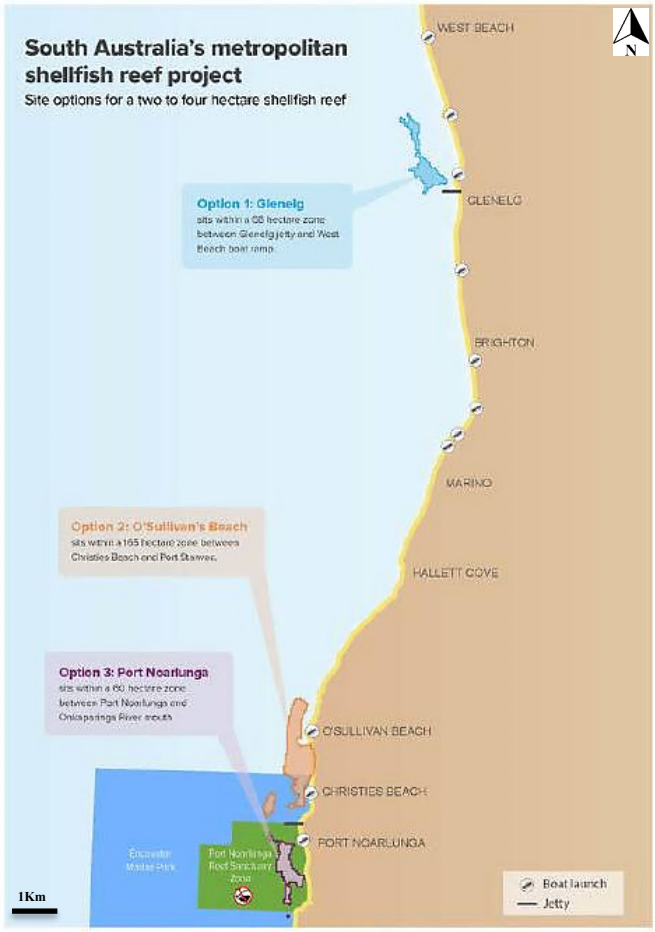

Figure 1: Three potential locations chosen by the State Government for the new shellfish reef.
Source: Department for Environment and Water 2020. (Reproduced under the CC-BY 4.0 license)

The public consultation for the selection of the three locations started the 20$^{th\ of}$ January 2020 and ended the 2nd of March 2020. The local community and stakeholders provided feedbacks, comments and voted for the most suitable location, according to their opinions, personal knowledge, and experiences; 654

respondents out of 1430 expressed Port Noarlunga as their preferred site, 484 indicated Glenelg, and 292 respondents out of 1430 voted for O'Sullivan Beach (Figure 2).

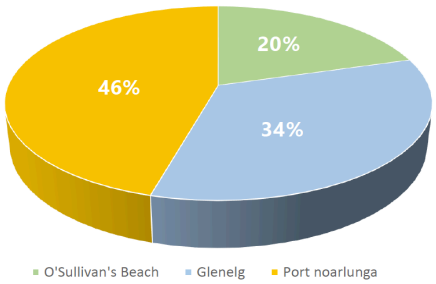

Figure 2: Results for the online survey taken by the public, to express their preferred site for the new South Australian shellfish reef. The percentages show how Port Noarlunga was the most voted location.
*Source: The Nature Conservancy and the Department for Environment and Water 2020. (*Reproduced under the CC-BY 4.0 license*)*

Although most of the involved stakeholders were in favor of implementing a new shellfish reef, several issues and concerns related to each of the three sites were expressed. Among the most common concerns, there were the ecological impacts of the new shellfish reef on existing ecosystems, the alteration of some surf spots in Port Noarlunga, potential impacts on local sea-bottom dynamics (sand shifting), the proximity to SA Water's wastewater treatment plan, with potential detection of contaminants, the vicinity to boat ramps, the amount of tourist and pollution in the areas and the potential impacts of the Patawalonga River (The Nature Conservancy and the Department for Environment and Water 2020). The final choice of location for the new shellfish reef was Glenelg (Figure 3); the Adelaide metropolitan coast project in Glenelg is based on the placement of different blocks of limestones, sedimentary rocks consisting of limestone. The new reef is the size of the Adelaide Oval, approximately 2-4 hectares, and it is located about one kilometre off the coast, at~ 10 metres depth (The Nature Conservancy 2020).

Picture removed due to copyright restrictions.

Original available online:

https://tnc.app.box.com/s/ml6xi7muh2x3ir7i1baj043hvs5k1n5y

Figure 3: Glenelg Beach. The yellow rectangle represents the location of the new shellfish reef. *Source: Rachel Bailey, The Nature Conservancy (2020).*

The project was completed at the end of November 2020, with goals and targets of the new shellfish reef restoration equally biological, ecological, social, and economic. The primary objectives include restoring the population of Australian native flat oyster (*Ostrea angasi*), the ecosystem services this species provides and

the reef's critical role in increasing the biodiversity of macroalgal species, fish, and other organisms (Gillies et al. 2018). From a socio-economic perspective, the new shellfish reef would be a key enabler for local businesses and fishing activities, both commercial and recreational, as well as for local citizens, schools, and universities, with activities and projects that enhance the public participation (e.g., citizen science and hands-on restoration) (The Nature Conservancy 2019).

1.2 Problem definition and importance of the project

South Australia has only recently completed (2018) its first shellfish reef restoration project, with the Windara Reef in the Yorke Peninsula, that represents the State's pilot project. The main goal of the shellfish reef restoration in South Australia is to increase the population of the native flat oyster (*Ostrea angasi*), which has been severely reduced due to the uncontrolled oyster fishing, since the 1900. Oyster and shellfish reefs are well known for the multiple ecosystem services they provide, which are essential for the maintenance and growth of various marine ecosystems. Shellfish reefs are also key elements for wave energy attenuation and shoreline stabilization, but that role is often underestimated or neglected. The extensive literature review done for this thesis identified the lack of available literature on the relationship between shellfish reefs with similar characteristics to the Glenelg Reef (e.g., depth and location from the shoreline), and the hydrodynamics affecting the marine environment. The current research is important because it provides primary results and information, on the role of the Glenelg reef on wave attenuation, throughout the use of numerical modelling, and it also gives an initial idea of the potential use of the Glenelg Reef as a sustainable resource for coastal protection.

LITERATURE REVIEW

1. Reefs: biotic and abiotic importance

Reefs consisting of multiple organisms, such as oysters, mussels, bivalves, corals, and other benthic organisms are among the most important marine habitats, from both biotic and abiotic perspectives. These reefs have a biological importance as nursery areas for a variety of marine species, ecosystem engineers, and they also offer protection from predation as well as other positive ecological effects for multiple marine species, from bivalves (e.g., oysters and mussels) to fish (Scyphers et al. 2011). Reefs can also advance local tourism and fishing activities (La Peyre et al. 2014).

From oceanographic and physical perspectives, shellfish reefs, such as oyster reefs have been identified as essential elements in sediment balance (Wiberg et al. 2019), by slowing down the shoreline erosion (Piazza et al. 2005), and by influencing the water dynamics (Dame and Patten 1981). Studies have shown how reefs have also a significant impact on water quality and on the mitigation of hazards affecting the coast, such as flooding and water overtopping (Ferrario et al. 2014). Finally, reefs situated offshore have been identified as elements of protection for the shoreline, its natural characteristics, and processes, but also for safeguarding the local tourism and economy, by improving the surfing conditions (Black 2001). Research conducted in the United States, particularly along the East coast and the Gulfs, highlighted how living shellfish reefs can provide benefits from a physical and engineering point of view (Morris et al. 2019). The relationship between physical features, such as structure's porosity, reef crest elevation and reef depth with the reef's ecological parameters, such as bivalve's growth rate, survival, and recruitment rate results as a primary element for reef success, in protecting the shoreline against erosion (Morris et al. 2019).

1.1 Shellfish Reefs

Oysters are bivalve organisms of extraordinary importance for multiple marine ecosystems, but also for local economies and fisheries. Oysters are sessile organisms considered "ecosystem engineers" (Gutiérrez et al. 2003). There are several species located in different habitats globally, where they form the shellfish reefs, which vary in size and form and predominantly consist of a single dominant species (Gillies et al. 2018). The number of organisms constituting the shellfish reef increases over time as other individuals and colonies are recruited, resulting in an ecosystem that provides a variety of services for other bivalve organisms, and several species of fish, such as nursery zones, refuge from predators and other biotic and abiotic factors, (McAfee et al. 2017; Crawford et al. 2019). On the other hand, shellfish reefs also provide a nutrient resource for several opportunistic and predatory species, because of the many species that identify the reefs as habitat and ecological niches. Oysters play a key role in balancing the physical and chemical characteristics of the marine environment; as filter-feeding organisms, they can filter suspended particles along the water column, resulting in the deposition of organic and inorganic material on the seabed, which

ensures the accretion of both the reef matrix and the organic component of the benthic sediment (Southwell et al. 2017). Shellfish reefs (Figure 4) have a key role on seagrass growth, they represent a suitable substrate for seagrass colonization and due to their ability to reduce water turbidity through filtration, they promote light penetration through the water column, resulting in increased growth rates of several species, such as *Posidonia oceanica*, predominantly found in the Mediterranean (Telesca et al. 2015) and *Posidonia australis*, found along the Eastern coasts of Australia (Gilby et al. 2019).

Picture removed due to copyright restrictions.

Original available online: https://www.nature.org/en-us/about-us/where-we-work/asia-pacific/australia/stories-in-australia/turning-rubbish-into-reefs/

Figure 4: Shellfish Reef at Georges Bay, Tasmania. *Source: The Nature Conservancy (2021).*

Since the early 1800s, in Australia, the most diffused local oyster species, the native flat oyster (*Ostrea angasi*) has been among the main products of oyster fishing, a type of fishery capable of severely impacting local shellfish reefs. Beck et al. (2011) estimated that 85% of global oyster shellfish reefs have been lost due to fishing and commerce of the species, with many oyster reefs considered functionally extinct. Today, shellfish reefs formed by *Ostrea angasi*, in southeastern Australia have been classified as "critically endangered" and included in the International Union for Conservation of Nature (IUCN) Red List of Ecosystems (Gillies et al. 2020).

1.2 Shellfish reef restoration

Shellfish reef restoration projects are extremely important for the rehabilitation and conservation of diverse oyster species which has been previously emphasized, with most of the nowadays available literature focused almost exclusively on the effects of shellfish reef restoration along U.S. coastal areas (McClenachan et al. 2020). Oyster reefs have been impacted by anthropogenic activities since the early 1900s, causing critical threats on their key role in controlling and balancing the natural physical processes in the marine environment, such as sedimentation and erosion (Housego et al. 2015). Over the past decade, the number of shellfish reef restoration projects has increased, but many of them failed due to factors such as hypoxic and anoxic conditions in the environment, diseases, very low larval recruitment rates (Powers et al. 2009), and sediment dynamics (Housego et al. 2015). Examples of a successful relationship between sediment dynamics and reef restorations are the projects implemented in the Great Wicomio River in Virginia (Schulte et al. 2009), where a total of 9 reef complexes were constructed in 2004, totaling 35 hectares, in area. The nine structures have two different ranges of heights, 25-45 centimeters for some of the units and 8-12 centimeters for the remaining reefs. Complexes with greater relief heights had a major success rate, with oyster population densities five-fold increase in three years, due to sedimentation rates (Schulte et al. 2009). In fact, reefs with greater height are less susceptible to sedimentation (Schulte et al. 2009), as more suspended

sediment is accumulated in the lower part of the water column, while deposition rates are reduced in the lower layers of the water column.

1.2.1 Shellfish reefs and restoration project in South Australia

Shellfish reefs consisting of the native oyster species *Ostrea angasi* used to play a primary ecological and economic role in South Australia, extending for about 1,500 km of coastline, from the Eyre Peninsula to Adelaide (Alleway and Connel 2015). Due to the exploitation of the resource through fishing activities but also due to disease and pollution, the situation in South Australia has exponentially worsened, with the 99% of shellfish reefs classified as "functionally extinct" (The Nature Conservancy 2019); Due to the ecological and economic importance of *Ostrea angasi*, South Australia started its first shellfish reef restoration project in 2014, with the Windara Reef restoration, South of the Ardrossan's coast in the Yorke Peninsula completed in 2018. The restoration plan proceeded with another shellfish reef in Glenelg, completed in 2020 and two further shellfish reef restoration projects in O'Sullivan Beach and Kangaroo Island. The purpose of the shellfish reef restorations in South Australia is to provide both habitats and nursery areas for key fish species, and to increase rates of denitrification, filtration along the water column, and sediment stabilization (The Nature Conservancy 2019).

1.2.1.1 The Windara reef

In 2014, the Government of South Australia announced the allocation of several million dollars for the promotion of tourism, creation of new marine parks, and enhancement of recreational fishing (Reeves et al. 2019). Of these funds, approximately $600,000 have been allocated for the restoration of the Windara shellfish reef, on the Yorke Peninsula (Figure 5a), with an initial deposition phase of a substrate, consisting of concrete and limestone blocks, totaling 4 hectares of surface area (Reeves et al. 2019), to be expanded up to 20 hectares, during phase two. In 2015, the Government of South Australia, along with Yorke Peninsula Council and The Nature Conservancy allocated additional funds to complete the Windara project, reaching a total of $3.7 million budget, part of which came from the Commonwealth Government National Stronger Regions Fund (Reeves et al. 2019). In total, approximately 10,000 tons of concrete and limestone structures were placed on the seafloor, for a resulting area equal to the extent of 11 Adelaide Ovals (Reeves et al. 2019). By 2019, there were already 80,000 oysters being deployed along the reef, with an additional 7 million in 2020. According to marine scientists from The Nature Conservancy and other institutions, such as the University of Adelaide and the Department of Primary Industries and Regions (PIRSA), oysters (Figure 5b) have successfully colonized the reef, with an average density of 674 oysters per square meter and a total of 6.1 million oysters in an area of 20 hectares (Reeves et al. 2019). Furthermore, additional positive effects of shellfish reef restoration have been identified, such as an increase in the number of marine species located on the reef, with multiple marine species reaching a population growth rate of 50-75% over the expected target, in the early stages of the restoration (Reeves et al. 2019). The local community has welcomed the reconstruction of the reef, with approximately sixty-five volunteers participating in events, surveys, and cleanup activities while, the Windara Reef was a central argument in national networks and local newspapers

(Reeves et al. 2019). Finally, an increase in the number of recreational fishermen has been seen in the area, mostly engaged in boating, or diving activities, with only a small number fishing in the reef areas, in compliance with the regulations that prohibit any type of commercial fishing and the capture of benthic organisms within reefs' zones.

Picture removed due to copyright restrictions.

Original available:
https://www.natureaustralia.org.au/what-we-do/our-priorities/oceans/ocean-stories/restoring-shellfish-reefs/gulf-st-vincent/

b

Figure 5: (a) Area of the Windara shellfish Reef in Gulf St Vincent.
Source: Yorke Peninsula Council (2015) https://yorke.sa.gov.au/discover/things-to-do/windara-reef/ (Reproduced under the CC-BY 4.0 license); (b) Windara Reef block of limestone, one year after deployment.
Source: Anita Nedosyko, The Nature Conservancy (2018).

2. Potential impacts of reefs on nearshore hydrodynamics

2.1 Tidal currents and wave-driven currents

The sea is a dynamic environment in constant motion due to the presence of tides, waves, and currents. The Moon and the Sun, due to their mass and gravitational attraction with other bodies lead to the movement of oceanic water masses, the so-called tides (Danovaro 2013). The tide is defined as a periodic movement of the sea determined by cyclically repeated mechanical forces, with a specific frequency, defined as "periodic" (Stride 1982). The Moon has a greater influence on terrestrial tides, while the influence of the Sun results in tides with half of the amplitude of the lunar tides. When the Sun, Moon, and Earth are aligned, during the new or full moon lunar phases, the gravitational forces of Sun and Moon add up and tides with maximum tidal amplitude alternate with events of minimum tidal amplitude; these tides are called spring tides and occur twice a month (Talley et al. 2011). When the Moon and the Sun form a 90° angle with the Earth, their respective gravitational forces oppose each other and lower-than-average tidal amplitude is created (Talley et al. 2011); these are called Neap tides and occur twice a month, during the first and last quarter of the Moon (Talley et al. 2011). Spring tides and Neap tides alternate (Figure 6), with two spring tides events and two Neap tides events during each lunar month. (Sumich and Pinkard-Meier 2016).

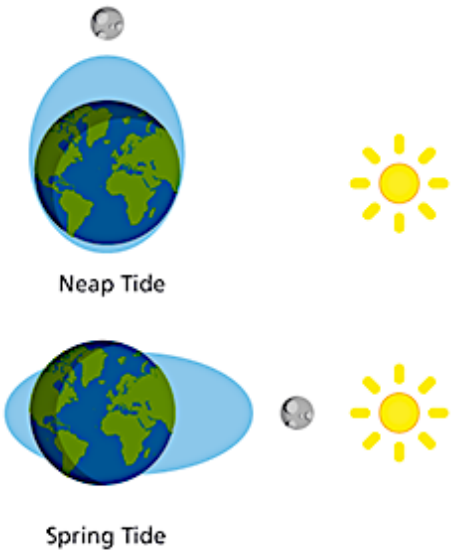

Figure 6: Spring Tides and Neap Tides
Source: Bureau of Meteorology (2021)
(Reproduced under the CC-BY 4.0 license)

There are then three other types of tides, diurnal, semidiurnal and mixed tides (Black 1986). Diurnal tides consist of one period of high tide and one period of low tide per day, semi-diurnal tides have two moments of high tide and two moments of low tide per day, and finally, mixed tides occur when every moment of high and low tide has different height (Black 1986).

The tidal excursion generates the tidal currents, consisting of horizontal flows of water masses having periodic movements, with rhythms approximately equal to the type of tide that initially generated them and that can therefore be semidiurnal, diurnal, and mixed (Carter 2013). The phenomenon is present in marine basins but also in large freshwater basins, estuaries, and channels. Tidal currents have lower magnitude in the open ocean, but they assume imposing forms when they affect channels, straits, estuaries or low and/or weakly inclined coasts, where they can reach speeds greater than 1 m/s (Masselink et al. 2014). There are two types of tidal currents, caused by the relationship between the tide's characteristics and the topographic characteristics of the seabed and/or coastline (Damiani et al. 2016). The rotary currents are currents typical of the open ocean and major depths, where the water masses do not meet obstacles. They are formed by the combined effect of the forces of attraction of the stars (Sun and Moon), with the Coriolis force and they occur with a continuous flow, different in speed, creating a rotary movement (Talley et al. 2011). Reversing (or rectilinear) currents are typical of coasts, estuaries, and fjords, they consist of an alternating movement of water masses in two possible directions, towards the coast (flood current) and towards offshore (ebb current) and they are separated by a period of slack water (NOAA 2021). The last type of tidal current are the hydraulic currents, where the movements of water, near lagoon inlets and/or isthmuses are found to have a velocity directly proportional to the square root of the water level difference between the two bodies (Damiani et al. 2016). Tidal currents can also be superimposed on other types of currents, such as gradient currents and wind-generated currents. Among the effects of the strongest tidal currents, there is the potential

erosion of coastal environments, with the formation of channels that penetrate inland, from the sea. The ebb and the flow of the tide, in the zone between low and high tidal levels (intertidal zone), gives rise to erosion, transport and redistribution of sediments both landward and seaward, forming a sedimentary environment: the tidal plain (Woodroffe 2002).

Another important phenomenon influencing the dynamics of coastal environments is wind and, consequently, waves and wave-driven currents. When the wind blows over the ocean surface, it causes stress on the ocean (wind stress), which in turn inputs the movement of water masses, up to a depth of 50 m along the water column (Talley et al. 2011). Different wind strengths and frequencies can result in persistent currents that characterize a specific given area, or mostly transient currents (Masselink et al. 2014). Wind is the main force behind wave formation (Black 1986); wave amplitude and frequency are influenced by the duration, intensity of the wind, and by the extent of the water surface over which the wind blows, called fetch (Danovaro 2013). When the wind begins to blow, the water surface appears slightly rippled, due to the formation of small capillary waves (Talley et al. 2011). Subsequently, wind-forced waves grow due to the pressure gradient between the back and the front of the wave, caused by the wind itself (Talley et al. 2011). Those waves are called surface gravity waves and they have a period between 1 and 25 seconds, while their wavelength varies between 1 meter and 1000 meters (Black 1986). Surface gravity waves move from offshore to the coast, where they break on the beach and for that reason, they can be classified as spilling breakers, plunging brakers or surging brakers (Talley et al. 2011), according to the morphological characteristics of the beach itself (Woodroffe, C.D. 2002). Spilling breakers are waves that break on a mildly steep beach, plunging brakers are typical of beaches with a medium steep and finally, surging brakers are those waves that break before reaching the shoreline, due to the characteristic high steep of the beach (Talley et al. 2011) (Figure 7).

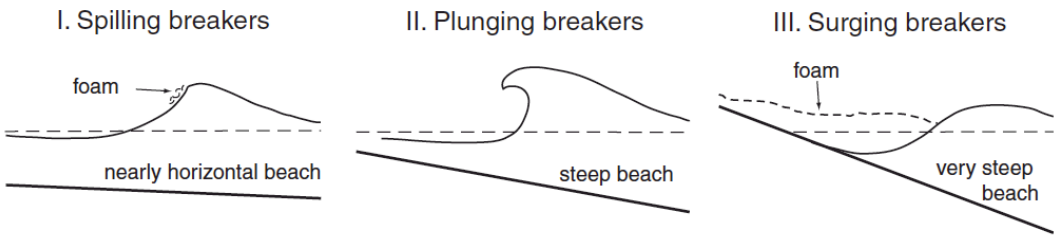

Figure 7: (I) Spilling breakers impacting a slightly steep beach; (II) plunging breakers in a moderate steep beach; (III) surging breakers affecting a very steep beach. *Source: Talley et al. 2011*. (Reproduced with permission)

When incident waves break, energy is dissipated along the surf zone and some of this energy generates nearshore currents, accompanied by sediment transport that gives morphological characteristics to the interested beach (Masselink et al. 2014). Nearshore currents are caused by a difference in gradient of mean water level, which is determined by dissimilarities in the breaking wave height and energy (Masselink et al. 2014). The intensity of those currents depends on the energy of the breaking waves and during extreme weather events, nearshore currents can result in the strongest currents, causing a high sediment transport.

There are three types of wave-driven nearshore currents: longshore currents, bed return flow or undertow and rip currents (Woodroffe 2002; Talley et al. 2011). Longshore currents occur parallel to the coast, within the surf zone and the wave that driven them have an obliquely oriented crest to the shoreline (Figure 8 (a)) (Masselink et al. 2014). The strength of longshore currents increases as the energy of the breaking wave grows, and it is also influenced by the angle at which the wave breaks on the shoreline (Masselink et al. 2014). The average speed at which longshore currents flow is about 1 m s^{-1}, although under strong wind conditions, the speed could significantly increase (Masselink et al. 2014).

Picture removed due to copyright restrictions.

Figure 8: (a) Longshore current flowing parallel to the coastline; (b) bed return flow/undertow, a current that moves vertically and towards the offshore, close to the seabed; (c) rip currents that flows seaward, creating channels within the surf zone. *Source: Masselink et al. 2014*.

The undertow or bed return flow is a current moving offshore (Figure 8 (b)), vertically and along the layer of the water column which is closer to the seafloor, and it balances the mass of water transported to the shoreline by the breaking wave (Talley et al. 2011). Bed return flow velocity varies between 0.1 m s^{-1} and 0.3 m s^{-1}, but with extreme wave conditions, it can reach 0.5 m s^{-1} (Masselink et al. 2014). Rip currents (Figure 8 (c)) are strong, narrow currents, with a velocity of 0.5-1 m s^{-1}, they transport water mass offshore, forming horizontal channels (Talley et al. 2011). The area in which rip currents form is influenced by the bathymetry and the morphological characteristics of the shoreline, while their intensity varies with the amplitude of the breaking wave, and they are usually absent under low wave conditions (Talley et al. 2011). The above-mentioned wave-driven currents do not occur separately from each other, but when waves break obliquely to the shoreline, both longshore currents and rip currents may be present (Masselink et al. 2014). When wind strength decreases, short waves give way to slower and longer waves called swells (Woodroffe 2002); swells vary in wavelength, they can reach tens of meters and they can propagate for quite long distances. An example are the swells that propagate for 4500 km circa, from the Gulf of Mexico to the northern coast of the Hawaii (Talley et al. 2011). If the wind direction remains constant for an extended period, such as a day or more, factors such as Earth rotation and the Coriolis force come into play (Black 1986). Among currents caused by prolonged wind, inertial currents result in clockwise movements of surface water particles, in the Boreal Hemisphere and counterclockwise movements, in the Southern Hemisphere; inertial currents are the result of the balance between the Coriolis force and the initially exerted wind force on the water surface (Talley et al. 2011). As the wind begins to blow stronger and for amore extended period of time, the influence of the Coriolis force increases, and the Ekman transport is formed (Talley et al. 2011). Ekman transport consists of the movement of water masses starting from the surface until a depth of about 50 meters, perpendicular to the wind direction (Talley et al. 2011). Surface currents move at a 45° angle to

the wind, due to the Coriolis force and the fluid dynamic resistance that is created between wind and water (Mann and Lazier 2013). The Ekman transport sees the ocean divided vertically into layers, with the current velocity decreasing from its maximum value, recorded on the surface to its minimum value, until the transport disappears at a depth of about 50 meters (Colling 2001). The direction of Ekman transport also shows a continuous slight shift in each successive layer to the right in the Northern Hemisphere and to the left in the Southern Hemisphere (Figure 9) named Ekman spiral (Knauss 2005). The water layer from the surface to the point of disappearance of the spiral is known as the Ekman layer (Talley et al. 2011).

Picture removed due to copyright restrictions. *Original available online*: https://www.offshoreengineering.com/education/oceanography/ekman-current-upwelling-downwelling **a**	*Picture removed due to copyright restrictions.* *Original available online*: https://www.briangwilliams.us/climates-weather/the-coriolis-effect-and-the-oceans.html. **b**

Figure 9: (a) Ekman spiral in The Northern Hemisphere; (b) Ekman Spiral in the Southern Hemisphere, showing the difference in the direction of the rotation. *Source: a) Offshore Engineering, 2021 and b) Brian Williams, 2021.*

Winds, together with pressure and density variations, resulting from different temperatures and salinities (Woodroffe 2002) is also the major force that triggers ocean movements on a global scale, by forming the currents that constitute the global ocean circulation (Black 1986).

II.I.I Effects of reefs on currents

The relationship between reef, wind and wave-driven currents was analyzed at the Ningaloo Reef, Western Australia, where a strong correlation was seen between tidal currents, longshore currents, and wave height, with the reef itself (Hearn and Parker 1988). The presence of a reef and its topographic characteristics have a major effect on breaking waves (Carter 2013) and consequently, on wave-driven currents. The influence of reefs on the hydrodynamics and morpho dynamics of coastal systems are most pronounced when reefs have a high roughness, and in some types of reefs (e.g., barrier reefs) by the presence of a lagoon (Carter 2013). The strong correlation between reefs and hydrodynamics is explored further in Symonds and Black's (2001) study of the John Brewer Reef, located in the Great Barrier Reef, 80 km north-east of Townsville, Australia. The John Brewer Reef is a shallow lagoonal reef that extends down to low-tide levels, from the 50 meters-deep continental shelf, it has a reef slope separated from the reef flat, by a lagoon that extends for about 300 meters in width and reaches a depth of 10-20 meters (Symonds and Black 2001). The currents affecting the reef are wave-driven currents and under calm weather conditions, the reef flat experiences currents with a peak of 0.1 m s^{-1}. Under increased wind conditions, when wave radiation stress grows by 2 or 3 degrees of magnitude (Symonds and Black 2001), conditions remain unchanged, due to the high roughness of the reef flat, which results in high bottom friction, when waves are present. As reef flat width and frictional resistance decrease, currents diminish, as seen as well at the Nusa Dua coral reef in Bali (Symonds and Black 2001); the results of both studies are consistent with the research done at the Ala Moana reef, Hawaii, where it was seen that a friction coefficient of C_f =0.16, resulted in high wave energy dissipation (Black and Gay 1988). As the friction coefficient, together with the substrate's roughness increases, there is a reduction in currents' strength, while a decrease in friction could lead to a 23 times greater current's force, affecting the John Brewer Reef (Symonds and Black 2001).

2.2 Sediment dynamics

Tidal-driven currents characteristics and their interaction with sediments have been studied since the 1970's; Piper (1978), through the analysis of sedimentary material dated about 3000 million years old has observed that tidal currents, of that period were stronger and that the tidal amplitudes were wider. One of the most important factors, affecting the energy of tidal currents is certainly the bathymetry of the seafloor (Stride 1982), which determines tidal resonance, characterized by extreme tidal amplitudes, shoaling amplification and energy loss due to the seafloor morphology (Stride 1982). The energy of tidal currents is dissipated due to bottom friction, and this determines a condition of "stress" with consequent movement and sediment transport. The above-mentioned process can be considered a feedback mechanism: the type of sediment (sand and/or gravel) transported by currents is related to the speed/energy of the current itself. At the same time, the speed/energy of the current is itself influenced by the bathymetry of the seafloor (Stride 1982).
The presence of structures on the seafloor, both artificial and natural in nature, such as coral and oyster reefs represents an additional element that directly affects the energy of currents and consequently, sediment dynamics (Franklin et al. 2013). A correlation exists between reefs and sediment dynamics, through a biunivocal mechanism, where the sedimentation rate influences the growth and survival rate of the reef and,

the reef itself can contemporaneously determine an effect on sediment transport and movement (Housego et al. 2015). As sediment grain size and current velocity vary, so does the response of the reef. According to the study by Housego et al. (2015), each grain size can be associated to a range of current velocity values, above which the shellfish reef can potentially be impacted by the sedimentation rate. If the water velocity is lower than the critical value for a specific grain size, the sediment concentration on the reef surface is lower and the reef survives and grows. In general, as sediment particle size increases, along with high velocity fluxes, a more favorable environment for oyster reefs survival and growth can develop (Figure 10) (Housego et al. 2015).

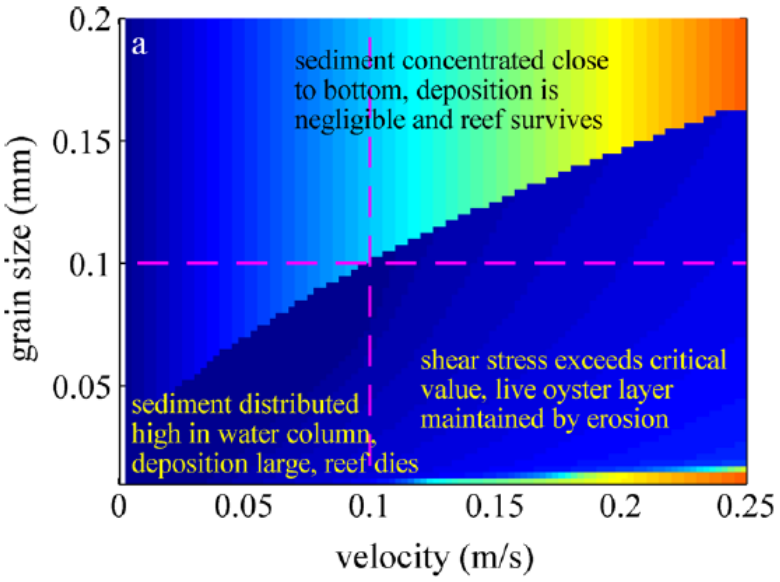

Figure 10: Different sediment deposition rates related to grain size and water velocity, showing how changes in values can potentially impact the reefs survival.
Source: Housego et al. (2016). (Reproduced with permission)

Sediment characteristics and dynamics influence reef ecology and physiology, and, on the other hand, reefs exert a key role, both on sediment dynamics and current flow, altering their characteristics due to their three-dimensional structure (Housego et al. 2015; de Paiva et al. 2018). Oyster reefs indeed have wave attenuation capabilities, and, in that way, they favor the sedimentation process and reduce the concentration of suspended sediment (Walles et al. 2016; de Paiva et al. 2018). In areas prone to erosion and sand deficit, the construction and/or restoration of shellfish reefs can be considered among the most common solutions for environmental protection (de Paiva et al. 2018). In a study carried out in the Netherlands, in the Oosterschelde Basin, an area prone to sedimentary deficit and erosion, 18 oyster reefs were constructed in 4 different zones. In zones with tidal flats subject to erosion, the EEE (Ecosystem Engineering Effect) of the oyster reefs increased sedimentation in the tidal flats by up to 3.60 centimeters per year, suggesting that the reefs had a positive effect on the accretion rate of the tidal flats.

2.3 Wave Attenuation

Reefs are particularly known to attenuate wave energy, especially in shallow and intermediate depth environments (Wideberg et al. 2019). To fully understand, the correlation between reefs and wave attenuation, Brown et al. (1999) give a specific definition of the above-mentioned phenomenon, which consists in the dissipation of wave energy with a consequent reduction in the wave height itself. The ways in which wave energy can be dissipated are different and they strongly depend on the type of wave, the wind speed/power, the frequency and height of the wave and the bathymetric characteristics of the area of interest (Wideberg et al. 2019). Franklin et al. (2013) carried out research in two phases, a laboratory phase, and a modeling phase, using COBRAS software (Losada et al. 2008), based on the study by Demirbilek et al. (2007), using the morphological characteristics (e.g., reef roughness and geometry) of the coral reef of Puerto Morelos, in the Yucatan Peninsula, Mexico. The obtained results showed that the presence of the reef, characterized by a specific roughness, influenced the reduction of wave energy and height by about 38%, compared to the control area, with the lowest roughness value (Franklin et al. 2013). The outcome of the research suggests that an increase in coral reef roughness represents a potential element of protection for the coastal environment (Franklin et al. 2013). For the intertidal and subtidal shellfish (oyster) reefs in New Jersey, Florida, and Louisiana, the data obtained in the analysis of the reef crest wave attenuation capability are similar for water levels 1cm below the reef crest, with approximately 83% of reduction of the wave energy, while with water levels 5cms above the reef crest, wave attenuation is only 42% (Morris et al. 2019). The reef crest elevation above/below the water surface can be added as a key factor in a reef's capability to attenuate wave energy, together with the orientation of the reef, the position of the reef and the depth of the water itself. (Black 2001). Results confirming the correlation between water depth and wave attenuation capacity of reefs were those obtained in Rahmshorn Bay, Virginia (USA), where four oyster reef restoration projects were in shallow estuaries and each reef had a crest elevation between 0.3-0.5 m below the mean sea level. Wideberg et al. (2019) analyzed the wave attenuation capacity of the four oyster reefs, under conditions of average wave heights varying between 0.03 m, 0.06 m, and 0.10 m, with peak heights of 0.3 m and 0.5 m, during winter months and an average water depth between 0.9 m and 1. 3m. The four shellfish reefs were able to reduce wave energy by 30-50% with a water depth range between 0.5-1.0 m and reef crest located 25cms below the water surface, while a slight increase in depth (1.0-1.5 m and >1.5m), diminished wave attenuation by 20% and 10% respectively. At deeper water conditions but in the presence of rocky platforms, with a higher roughness value, the reduction in wave energy and height increases dramatically, as seen by Poate et al. (2016) in four different areas between England and Ireland. At depths ranging between 0.5m and 6.8m, rocky intertidal platforms with variable morphology and wave heights oscillating between 0.5m and 1.9m, there was a decrement in wave height with subsequent wave breaking (Poate et al. 2016). Specifically, two of the sites analyzed, Portwrinkle and Lilstock experienced a decrease in wave height from 1.2m to 0.7m, with Portwrinkle's reef being smaller in size but having a greater roughness value (Poate et al. 2016). The results obtained by Poate et al. (2016) are consistent with those of Franklin et al. (2013), with reef roughness values being a key element in reducing energy and wave height.

2.4 Coastal protection and reef effects on coastlines

Reefs and their ecosystem services, in particular wave attenuation and sediment trapping capability are key features for the protection of coastal environments and are considered a sustainable solution for erosion control and coastal defence (Borsje et al. 2011). There are numerous benefits provided by coral and oyster reefs worldwide in terms of erosion control, flood control, wave attenuation, and coastal infrastructures protection (Figure 11) (Narayan et al. 2016).

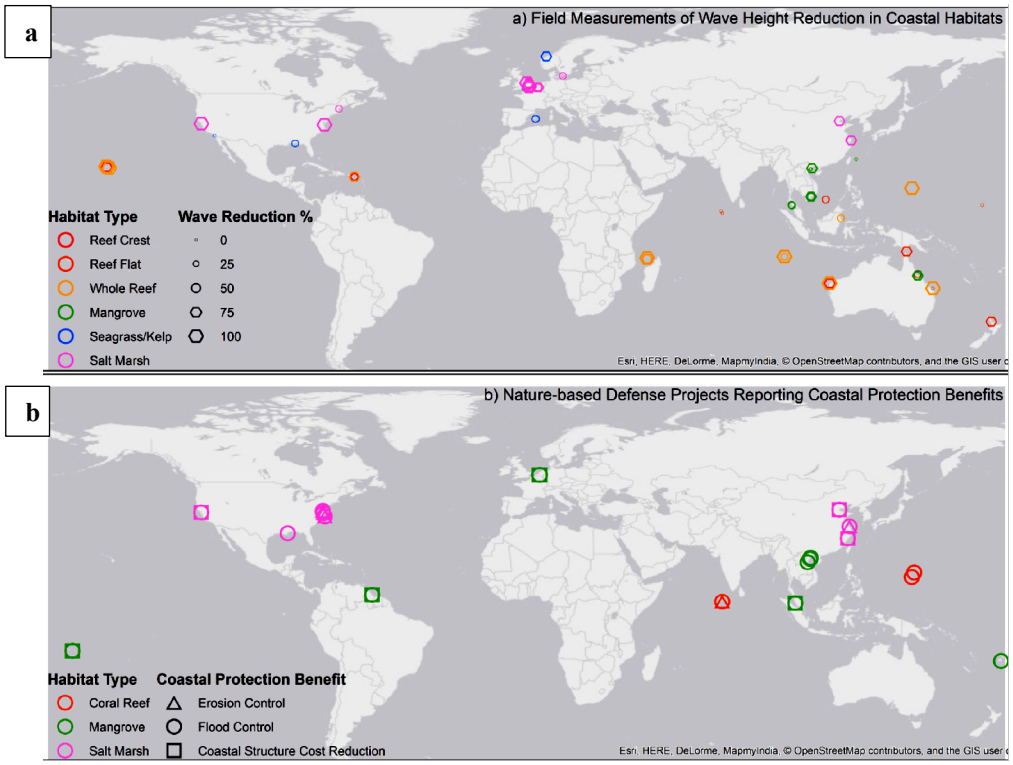

Figure 11: (a) Map of wave attenuation by natural defences including reefs; (b) benefits of coastal protection from natural environments/reefs restoration project. *Source: Narayan et al. 2016*. (Reproduced under the CC-BY 4.0 license)

Reef-building species as ecosystem engineers can modify the surrounding environment, both from a hydrodynamic and sedimentary point of view (Van Leeuwen et al. 2010). This capacity of habitat modification (Borsje et al. 2011) has been verified with a pilot restoration project in the Netherlands (De Vries et al. 2007), involving the construction of an oyster reef in large intertidal flats. Results showed that the presence of oyster reefs contributed to the attenuation of hydrodynamic energy and the accumulation of muddy sediment (De Vries et al. 2007 as cited in Borsje et al. 2011). The results obtained by De Vries et al. (2007) (Borsje et al. 2011) are consistent with studies in the northern United States, such as that of Piazza et al. (2005), in the Terrebone basin (Gulf of Mexico), Louisiana. The American site is characterized by the presence of wetlands, a high rate of subsidence (0.6-1.1 meters/year) and wetland loss rate of more than 2,500 hectares per year (Barras et al. 2003). Two shorelines were selected as study sites, one with low energy hydrodynamic features, the other located in a high wave energy environment. For each of those shorelines,

six sites were analysed, three with reefs, or “culched” and three control sites without reefs, or “non-culched” (Piazza et al. 2005). Each experimental oyster reef was 25 meters long, 1.0 meter wide, placed 70 cm deep and 5 meters from the shoreline. The results showed a shoreline retreat rate of 0.07-0.08 m/month for the reef-affected area, from June 2002 to June 2003, while at the control sites, the monthly shoreline retreat rate was 0.12 m/month (Piazza et al. 2005). However, the study also showed that in areas with high hydrodynamic energy and with two storm events in October and November 2002, the shoreline retreat data (0.14 m/month) suggested no benefit from the oyster reef in protecting the area (Piazza et al. 2005).

The use of submerged offshore artificial structures has also proved to be successful in protecting the coastal environment, particularly in preventing shoreline erosion and by increasing sedimentation (Turner, 2006). At Narrowneck, Gold Coast (Queensland, Australia), a “V”-shaped artificial reef, made with geotextile structures was constructed in the second half of 1999 (Figure 12), with a total distance of 600 meters from the shoreline, a size of about 350 meters along the coast and positioned between 2 meters (shallowest part) and 10 meters (deepest part) depth (Ranasinghe and Turner 2006).

Figure 12: The Artificial Surf Break in Gold Coast, Queensland (AU). The artificial reef presents a “V” shape, with the apex pointing seaward. *Source: Courtesy of the International Coastal Management, Australia,* www.coastalmanagement.com.au *(Ranasinghe and Turner, 2006)* Reproduced with permission.

The Gold Coast is characterized by high energy beaches, with the Narrowneck shoreline having a sediment movement rate of approximately 500,000 m^3 per year northward and 150,000 m^3 per year southward (Ranasinghe and Turner 2006; Turner 2006). In addition, Narrowneck is prone to sporadic extreme weather episodes that have previously damaged properties, infrastructures, and beaches themselves (Turner 2006). In the first 12 months, after the completion of the first phase of reef implementation (January 2002), a 25 meters increase, in width of the southern zone of the beach was seen, for 450 meters alongshore, while for the northern part of the area, the width increase was 10 meters for the northern shoreline, for approximately

400 meters along the coast (Ranasinghe and Turner 2006; Turner 2006). After the completion of two following phases of the artificial reef construction, in January 2003, results showed a shoreline width growth of additional 10-20 meters compared to years prior the reef construction in the same period (January) and same area of interest (Turner 2006). The results presented by Ranasinghe and Turner (2006) and Turner (2006) are in line with those seen by Weppe et al. (2009) for the artificial reef at Mount Maunganui, New Zealand. The Mount Maunganui reef consists of several geotextile containers, it has a characteristic "V" shape, and its construction went from 2005 to 2008 for research purposes (Weppe et al. 2009). The reef is a submerged structure, located 250 meters from the coast and it has a width of about 80 meters alongshore (Figure 13).

Picture removed due to copyright restrictions.

Original available online:
https://www.nzherald.co.nz/bay-of-plenty-times/news/mounts-artificial-reef-to-be-removed/GA44JIIW7LW5P457SBPXO5PKYU/

Figure 13: The Mount Maunganui Reef in New Zealand. *Source: Bay of Plenty Times (2014)*

However, the Mount Maunganui area, unlike the Gold Coast is an area of low hydrodynamic energy, with wave heights usually less than one meter (H<1) and sporadic subtropical storm events (Pickrill and Mitchell 1979). In the period prior to the reef construction (August 2004-November 2005), it was found that there was a gradient of sediment transport from northwest to southeast along the shoreline, with a net sedimentation rate of 60 000 m3 - 80 000 m^3 per year, in the south-eastern part of the beach (Healy 1980). Following the construction of the artificial reef, two effects were highlighted: a more crenulated shoreline, with an irregular outline in the area centrally facing the reef, and a "groin effect", with the accumulation of sediment and the formation of a salient, which resulted in a net shoreline of about 20 meters, for 150 meters along coastline, in the north-west direction. The Narrowneck and Mount Maunganui artificial reefs can then be identified as having an important effect on shoreline changes and response, to the presence of offshore submerged structures (Weppe et al. 2009).

2.5 Benefits of reefs in case of extreme weather events

The capability and importance of reefs and other coastal systems in protecting the shoreline and the coastal environment are critical, especially in areas prone to extreme events, such as flooding, hurricanes and storms. Those are only some examples of the catastrophic events whose risk has been dramatically increased by the escalation of coastal anthropogenic activities and effects of climate change, such as sea-level rise (SLR) (Reguero et al. 2019). The state of Quintana Roo, Mexico presents one of the most exploited coasts worldwide, where since the 1970's, there have been numerous coastal development projects (Reguero et al. 2019) and a population of approximately 1.5 million, mostly located along the coast. The state's coastline is faced by The Mesoamerican Reef (MAR) (Figures 14 and 15), the largest reef in the entire western hemisphere (Reguero et al. 2019).

Picture removed due to copyright restrictions.

Original available online:

https://www.islandlifemexico.com/mesoamerican-barrier-reef/

Figure 14: Aerial view of the Mesoamerican Reef (MAR) in Quintana Roo, Mexico. Source: Island Life Mexico, 2021.

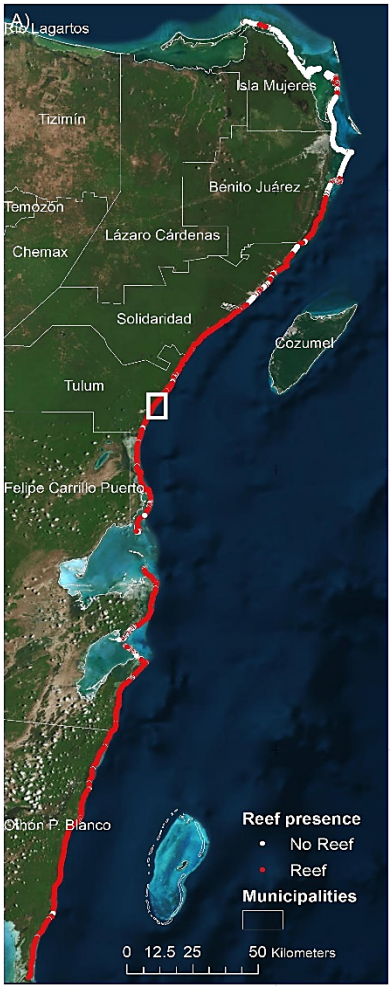

Figure 15: The Quintana Roo coastline; the red line is the reef along the coast, the white line represents the area without the reef. *Source: Reguero et al. 2019.* (Reproduced under the CC-BY 4.0 license)

Quintana Roo is an area frequently subjected to storms and strong hurricanes, such as Hurricane Emily (2005), Hurricane Wilma (2005), and Hurricane Dean (2007). Using CLIMADA and XBeach software, Reguero et al. (2019) simulated about 1500 storms, based on meteorological data from about 900 past storm events. The results obtained with the simulation of the same conditions experienced during hurricanes Emily (category 4), Wilma (category 5), and Dean (category 5) showed that the MAR resulted in 43% less flooding damage rate in the area for Hurricane Dean, while for hurricanes Wilma and Emily the percentage of flooding damage reduction rate was 11% and 9%, respectively. Data for hurricanes Wilma and Emily were substantially lower due to two main factors: the two events affected mostly the northern part of the country, where the reef presence was scarcer and there was no direct protection (Figure 15), and in addition, Emily and Wilma were characterized by extreme rainfall events (Escalante-Mancera et al. 2009; Silva et al. 2009 as cited in Reguero et al. 2019). Overall, the quantification of benefits and protection of the coastline, the population, and the infrastructures by the MAR during the extreme weather events of 2005 and 2007 was estimated to reach the 34.6% for Hurricane Wilma and 92% for Hurricane Dean (Reguero et al. 2019).

The positive influence provided by reefs to coastal environments during storms was highlighted also during extreme weather events of lower intensity, such as those regularly recurring in Yanchep (Figure 16), a lagoon region of Western Australia (Gallop et al. 2012). The beaches at Yanchep are typically sandy and the environment is microtidal, with a semidiurnal tidal range of 0.165 meters. Storm events numbered approximately of 30 per year, occurring among 1 or 2 days in July, with strong north-western winds and waves that range in height from 1.5 meters to 2 meters (Lemm et al. 1999). During storms, the direction of net sediment transport undergoes a reversal; it normally occurs alongshore from south to north during summer and spring months, whereas during extreme weather events, the net sediment transport varies from north to south (Gallop et al. 2012). Three different profiles of the perched beach were identified along the Yanchep coast, based on topographic features (Figure 17): the first profile, the Exposed Profile, with its submerged part made of sandy substrate, a Reef Profile facing limestone reefs located at 3 meters depth and a Bluff Profile, where the emerged part of the beach was connected to a limestone promontory, emerging above the water level.

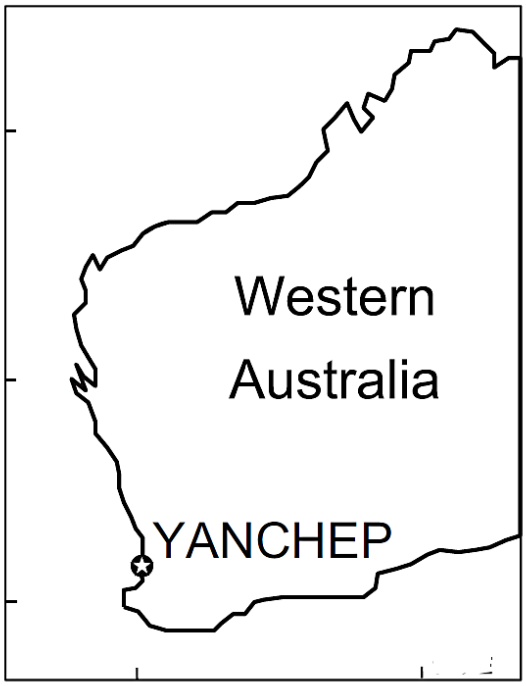

Figure 16: Yanchep in Western Australia. *Source: Gallop et al. 2012* (Reproduced with permission)

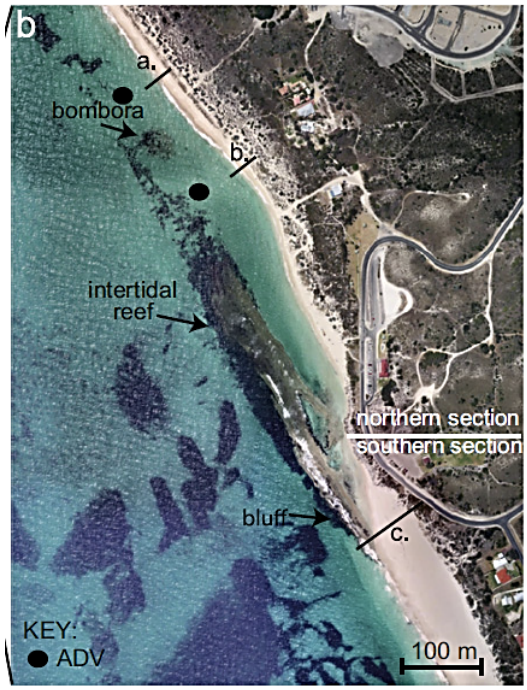

Figure 17: The three Yanchep beach profiles. (a) the Exposed Profile; (b) the Reef Profile; (c) the Bluff Profile. *Source: Gallop et al. 2012* (Reproduced with permission)

During two storm events with the first occurring from July the 8th 2010 to July the 10th 2010 and the second occurring from July the 11th to July the 13th 2010, the Exposed Profile experienced erosion, with the sediment accumulating to form a steep scarp of approximately 2 meters. The Reef Profile experienced minor erosion and in fact accretion, which balanced out the previously seen erosional events, while the Bluff Profile experienced slight accretion at the top of the beach face and acquired a greater degree of slant (Figure 18) (Gallop et al. 2012).

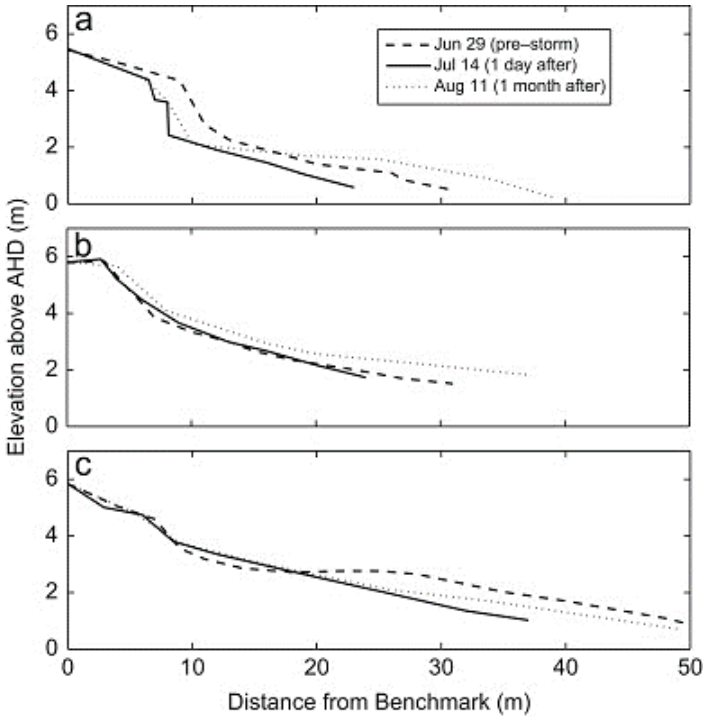

Figure 18: (a) Exposed Beach Profile, one day after and one month after the storm; (b) The Reef Profile, one day after and one month after the storm; (c) The Bluff Profile, one day after and one month after the storm, showing the formation of a 2 meters-high scarp and erosion in the Exposed Profile, a mild change in profile volume for the Reef Profile and a severe change in slope for the Bluff Profile. The dashed line represents the three Profiles before the storm event, the continuous line is 1 day after the event and the dotted line represents the situation, one month after the storm event. *Source: Gallop et al. 2012.* Reproduced with permission.

The beach profiles underwent several morphological changes during the July 2010 storms, with episodes of erosion and accretion of different intensity, in distinct areas of the shoreline where in some cases, accretion occurred just 10 meters away from where erosion was seen (Gallop et al. 2012). In general, the responses of the three profiles to the two storms were diverse, resulting in a greater vulnerability to storm erosion by the Exposed Profile, which was completely eroded the second day (13th of July 2010) of the second storm event. At the same time, the Reef Profile has been identified as the most stable profile, with no change in volume; furthermore, the Reef Profile has experienced the highest rates of accretion, reaching a greater volume than pre-storm periods, with a recovery rate bigger than the two other profiles (Figure 18). The Bluff Profile had specific morphological characteristics that made it less prone to erosion but despite those features, it was moderately eroded and also had the slowest recovery rate after a month from the two extreme weather events (Figure 18) (Gallop et al. 2012). In conclusion, both the Quintana Roo and the Yanchep studies underlined how the presence of reef structures has guaranteed the reduction in damage to infrastructures and severe impacts on the population, by having positive effect on both physical and economic key elements, and also protection and preservation of the shoreline's morphological characteristics and morpho dynamics.

3. Modelling reef impacts on the hydrodynamics: Delft3D

Numerous studies (Lesser et al. 2004; Lowe et al. 2009; Villanoy et al. 2012; Hardy et al. 2020) have used Delft3d software as a fundamental resource for the development of 2D/3D models, to analyze sediment dynamics and hydrodynamics within diverse types of reefs, both in standard weather conditions and extreme weather events, proven the software to be a valuable instrument to validate field acquired data. Delft3D is an open-source 3D modeling software developed by the Deltares research center in the Netherlands and it is widely used for the study of sediment transport, water quality and morphological characteristics of river, estuarine and coastal environments (Deltares 2014). Delft3D FLOW represents the main component of the Delft3D software, and it can simulate the hydrodynamic and sedimentary characteristics of given areas, under specific meteorological and morphological characteristics (Deltares 2014). Another fundamental module of the software is Delft3D WAVE that simulates wave propagation, wave generation by winds, wave-wave interaction, dissipation, and refraction (Villanoy et al. 2012), through the incorporation of information related to sea-bottom topography, winds, water level and currents in both shallow and deep environments (Deltares 2014b). Lesser et al. (2004) have previously analyzed the use of Delft3D FLOW and Delft3D WAVE for the simulation of the most common processes in coastal environments and the software has been shown to be valid for the simulation of sediment transport processes, sediment concentrations in the water column, and wind-driven currents effects (Lesser et al. 2004). Delft3D FLOW has also been used to study turbulence caused by suspended sediment in the water column, changes in sediment transport, and erosion (Lesser et al. 2004), in a study based on a series of laboratory dataset. Delft3D has also been proved successful for real-life environmental studies, such as the study at Kaneohe Bay, Oahu, Hawaii by Lowe et al. (2009), using Delft3D to develop a model with specific conditions of waves and currents, and compare them to field measurements. The Oahu area records a massive presence of coral reefs along the northeast coastline, with a length of about 6 km and 2 km wide, located at 3 meters depth. Between the shoreline and the reef, there is a small lagoon, about 1-2 km wide and 10-15 cm deep where coral patches can be found emerging at 1 meter from the water surface (Figure 19).

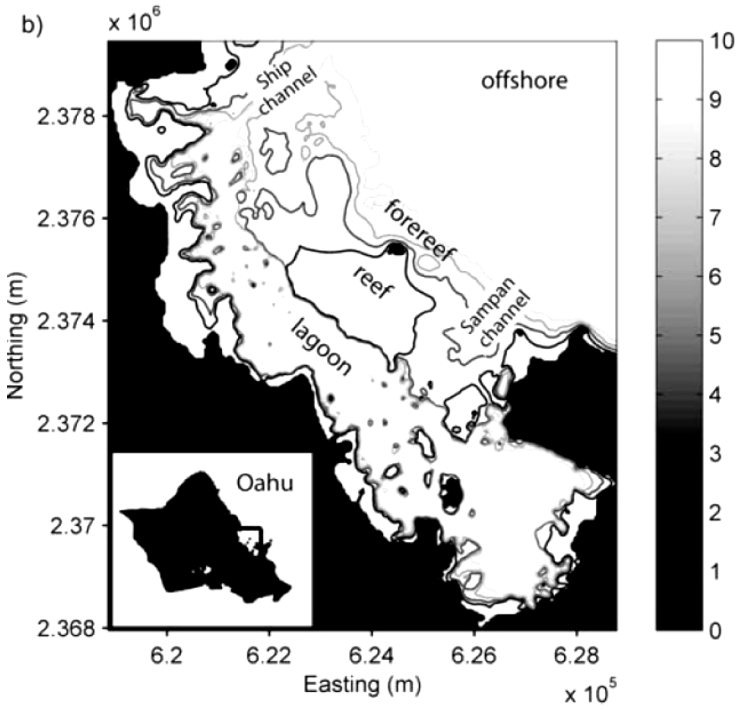

Figure 19: Aerial view of part of the north-eastern Oahu coast. It can be seen the lagoon between the shore and the reef, together with several smaller coral patches in the lagoon. *Source: Lowe et al. 2009*. Reproduced with permission.

The computations with Delft3D were conducted on a timeframe of 4 weeks, from January 24th to February 18th, 2006. Wave and current data were measured in seven different areas (Figure 20) of the forereef (W1 and W2), the flat reef (A2, A3, A4) and the back reef (W3 and W4), every hour, using four wave pressure gauges and three ADCPs. According to Lowe et al. (2009) the SWAN model (Delft3D WAVE) returned results consistent with the data collected by the deployed equipment, especially for the wave height parameter (Figure 21 and Table 1), despite some shortcomings such as a smaller prediction for current changes on the reef flat. In general, the use of Delft3D and 2D/3D numerical models is an advantageous tool for morphologically complex environments, with multiple hydrodynamic mechanisms (waves and tides) and for reef-lagoon coastal systems and rocky shorelines (Lowe et al. 2009).

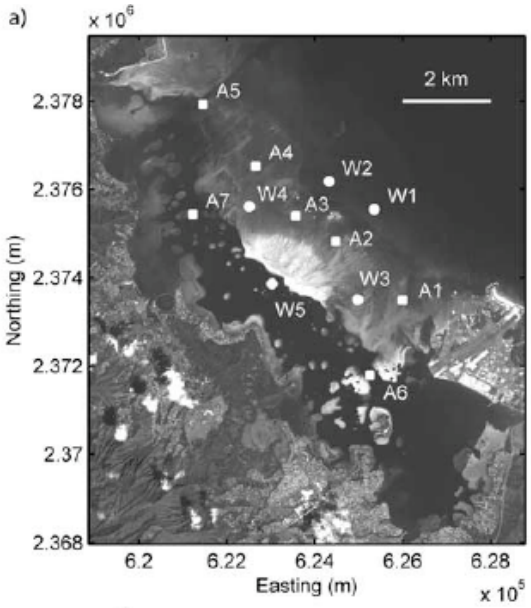

Figure 20: Sites were wave and current data were measured in the Kaneohe Bay, Oahu, Hawaii. Sites W1 and W2 are located at the forereef, A2, A3, A4 at the reef flat and W3 and W4 are at the back reef. *Source: Lowe et al. 2009*. Reproduced with permission.

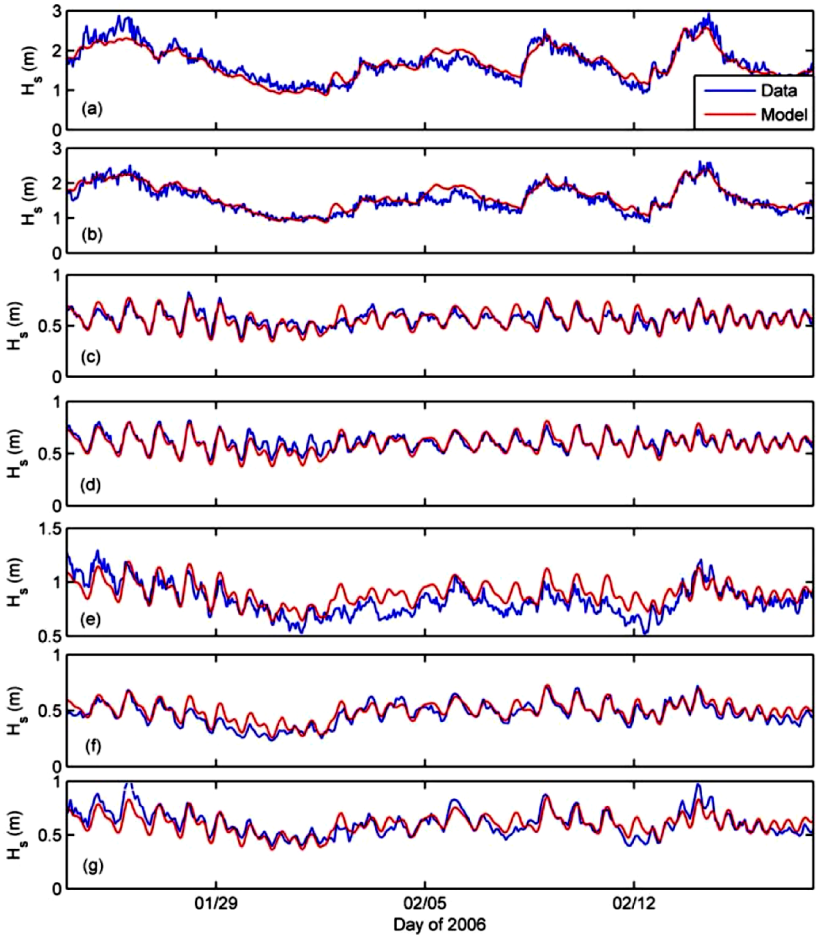

Figure 21: Comparison between model and equipment data, related to wave height (Hs); (a) and (b) on the forereef; (c), (d) and (e) on the reef flat; (g) at the back of the reef. The Figure shows the observed significant wave height (H_s) in blue and the modelled H_s in red, for the seven sites at the forereef, reef flat and back reef. *Source: Lowe et al. 2009.* Reproduced with permission.

Table 1: Wave height (H_s) measured by wave gauges and ADCPs compared to SWAN outputs. *Source: Lowe et al. 2009*.

H_s (m) (Mean SD)		
Field	Model	Skill
1.69 (0.44)	1.67 (0.40)	0.96
1.54 (0.38)	1.60 (0.37)	0.96
0.57 (0.08)	0.56 (0.09)	0.93
0.61 (0.08)	0.60 (0.09)	0.94
0.84 (0.14)	0.90 (0.11)	0.81
0.47 (0.10)	0.50 (0.09)	0.93
0.61 (0.11)	0.60 (0.10)	0.89

Hardy et al. (2020) also conducted research in the Hawaiian archipelago, more specifically at the Kaanapali Beach, Maui. Hardy et al. (2020) used Delft3D for analyzing sediment transport and the morphological changes, from January 2016 to February 2016. Both the Delft3D FLOW and Delft3D WAVE modules were used concurrently to obtain results for sediment and physical changes, with data from the software "satisfactorily in accordance" with previously made observations (Hardy et al. 2020).

Numerous studies have used Delft3D FLOW and WAVE to investigate the relationship between reefs, wave attenuation and sediment dynamics, with encouraging results even in the simulation of extreme events (e.g., storms and hurricanes) (Villanoy et al. 2012). The study of Villanoy et al. (2012) analysed storm-generated waves and the effect of a coral reef ecosystem in Sorsogon, Philippines, an area highly prone to extreme weather events, with past episodes of category 4 and category 5 hurricanes. Two areas along the Sorsogon coast were investigated, Bagacay and Rizal located on the southeast and northeast of the archipelago respectively, both facing coral reefs at about 2 meters depth, and having interconnective channels, where the reef presence is nil and the coast exposed (Figure 22) (Villanoy et al. 2012).

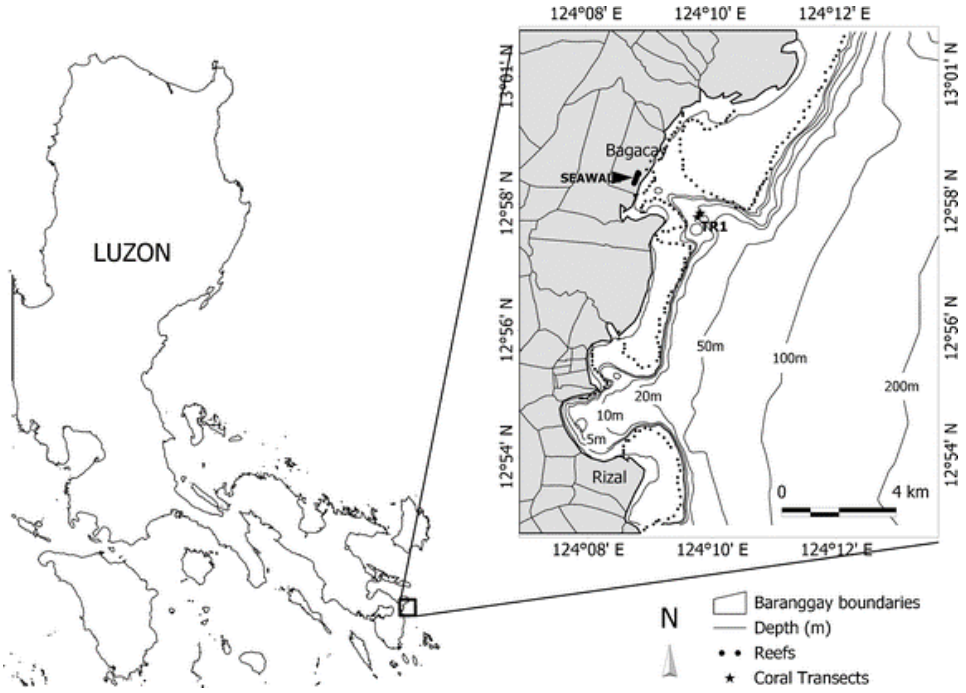

Figure 22: Map of the study area, with the right-side box showing the bathymetry and the location of the coral reefs. *Source: Villanoy et al. 2012.* Reproduced with permission

Seven Delft3D WAVE computations (A to G) were performed, with different wind, significant wave height and sea level rise conditions, taken from the QuickSCAT satellite database and related to the period 2000-2009. For each one of the computations was specified the presence/absence of characteristic monsoonal winds, the significant wave height, variable from 2 to 4 meters (example of Computation A in Figure 23), the wave period of 8 seconds and, for two of the runs, a sea level rise value of 0.3 meters and 1.0 meters (Villanoy et al. 2012).

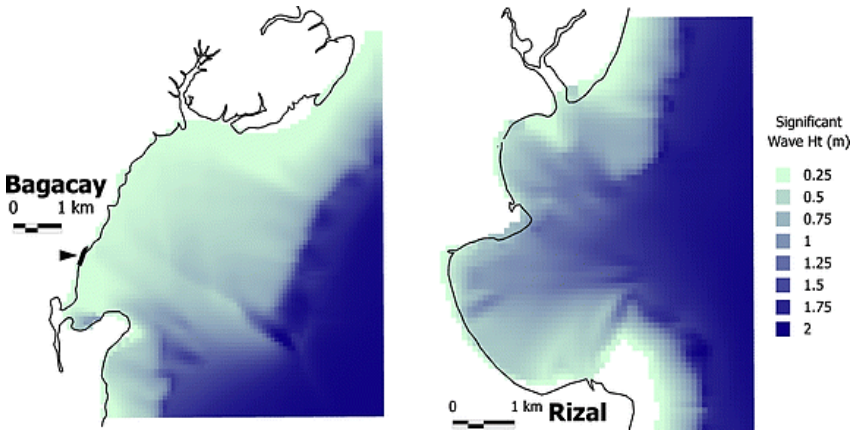

Figure 23: Significant wave height along the coast of Bagacay and Rizal for Delft3D WAVE model A computation, with wind forcing of 10 m/s NE, no sea level rise and presence of corals. *Source: Villanoy et al. 2012.* Reproduced with permission.

The results of the seven Delft3D computations showed that the presence of a coastal reef system results in an increased wave energy dissipation and a decreased wave run-up on the shoreline. The models also showed that wave attenuation occurs both with and without sea level rise.

AIM AND OBJECTIVES OF THE RESEARCH

The aim of this research is to analyse the potential for the Glenelg shellfish reef restoration to cause wave energy attenuation, given its distance from the shoreline and its bathymetry, using a numerical modelling. The proposed aim will be attained with the achievement of three main objectives:

- Analysis of data provided by SA Water, measured by ADCP from the 26th of March 2021, 9:00am to the 16th of April 2021, 1:00pm, related to significant wave height (*Hm0*), peak period (*Tp*) and mean direction (*MeanDir*), with identification of "*calm*" days (<*Hm0*) and "*storm*" days (>*Hm0*)

- Use of the software Delft3D (Flow and Wave) for the development of a numerical model to simulate the hydrodynamics in the study area.

- Validation of the model: comparison between the data obtained from the computation and data related to significant wave height (*Hm0*) collected by pressure sensor and provided by SA Water. Finally, a process of model validation will be performed to verify the accuracy of the simulation results.

METHODS

This section aims to describe the main environmental characteristics of the study area, the field methods and the numerical modelling employed in this study.

1.1 Study Area

The area on where the Glenelg Shellfish Reef is located is part of the eastern side of Gulf St Vincent (Figure 24), one of the two Gulfs of South Australia, together with Spencer Gulf. Gulf St Vincent is characterized by a surface area of 6.8 x 10^3 km^2 and a relatively shallow mean depth of about 21 meters (Bye 1976), with limited water exchange with the Southern Ocean.

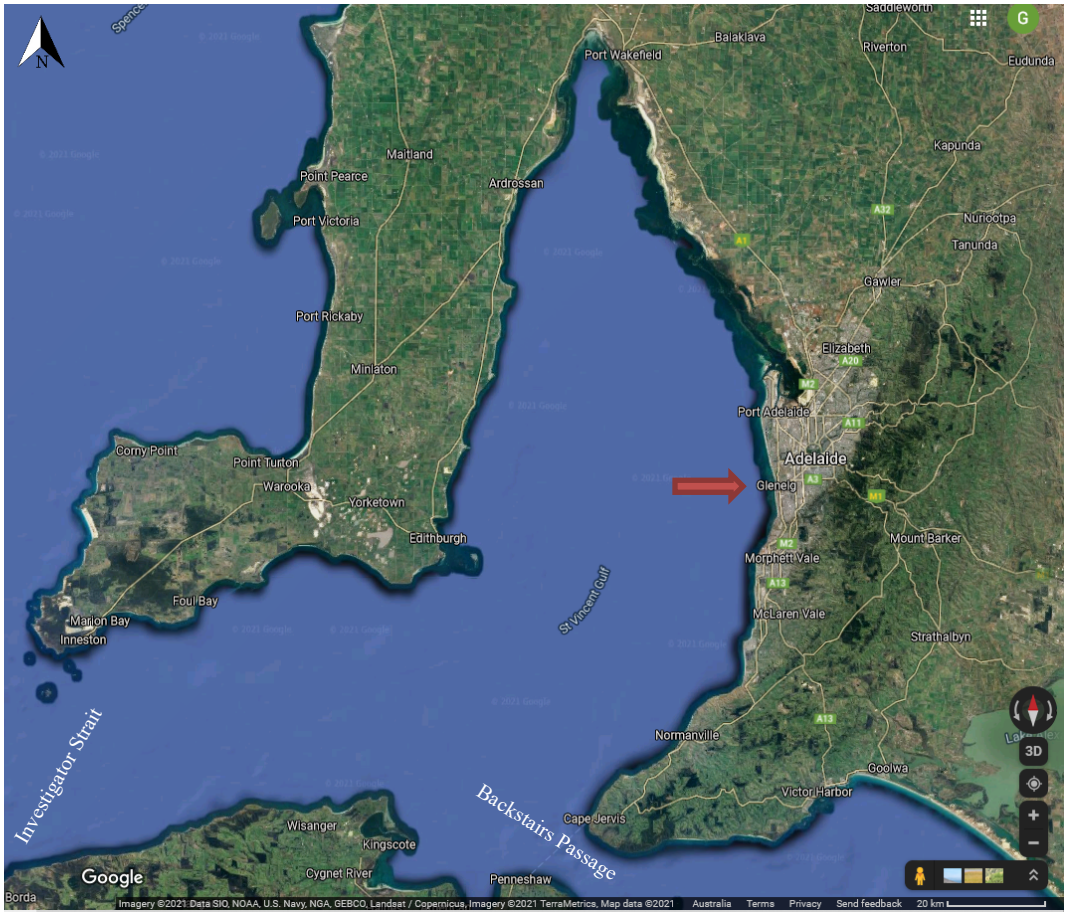

Figure 24: Gulf St Vincent. The arrow indicates the approximate position of the Glenelg Shellfish Reef. Source: Google Maps (2021). Reproduced with permission.

Incoming currents from the Southern Ocean enter the Gulf from the Investigator Strait, while the outflow passes through Backstairs Passage, with the water mass circulating in a clockwise direction (Bye and Kämp 2008). The two Gulf St Vincent's Straits (Investigator Straits and Backstairs Passage, Figure 24) have the role of blocking swells from the Southern Ocean, which have the greatest effect in the coastal areas within the Gulf. The dominant winds are from South-West, although occasionally, strong north-western winds

operate in the area (Bye, J.A. 1976). The St. Vincent Gulf can be classified as having a microtidal to a mesotidal range, between 1.2 to 3.3 meters (Bryars et al. 2016), with a low-energy environment prevailing in the upper parts of the Gulf (Bourman et al. 2016). Tides run parallel to the coastline, proceeding towards the northern end of the Gulf. This tidal flow is followed by a slack water phase and then, tides reverse by proceeding southward, with an outgoing tidal flow (Grzechnik and Noye 1999). The area can also be affected by storm surge, which can increase water levels of~3.5 meters, above the astronomical tide (PIRSA 2017). The area where the Glenelg shellfish reef is located, as well as the Adelaide metropolitan coast, is affected by a mixed semidiurnal tide, where two low tides and two high tides occur in 24 hours, with different heights (Figure 25).

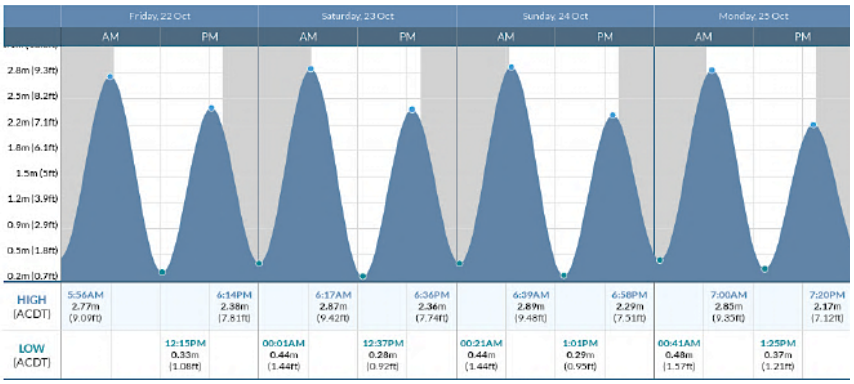

Figure 25: Example of mixed semidiurnal tidal range for the city of Adelaide. The chart shows the height and time of high tide and low tide for Port Adelaide. The grey bars correspond to nighttime hours, occurring between sunset and sunrise in Adelaide. Source: Tide-forecast.com (2021), available at https://www.tide-forecast.com/locations/Port-Adelaide-Australia/tides/latest (Reproduced with permission).

The nearshore habitat along the Adelaide coast is predominantly constituted by seagrass in the Northern part of the coast, due to low wave energy, and on the other hand, the metropolitan south coastline is rich in rocky substrate, where the wave energy is higher. Despite the predominance of seagrass along the northern metropolitan coast, since the 1920s a process of large-scale decolonization has begun, accompanied by a degradation of rocky reefs along the North coast, due to increased coastal development, discharges from industries, stormwater runoff and consequent reduced water quality (e.g., increased nitrogen) (Edyane 1999).

1.2 Field Methods

Two pressure sensors (RBR*solo*^{3}DWave16) were used to measure significant wave height (*Hs*) and peak period (*Tp*), while an ADCP (Nortek Aquadopp) was deployed to include mean wave direction (*MeanDir*) measurements within the Glenelg shellfish reef, as key parameters for the following modelling phases of the project. The ADCP provides information on *Hm0* (spectral significant wave height), which can overestimate the significant wave height (*Hs*) by approximately the 5%. The instruments were deployed South-West and North-East of the reef, at a distance of 100 meters from its centre (Figure 26).

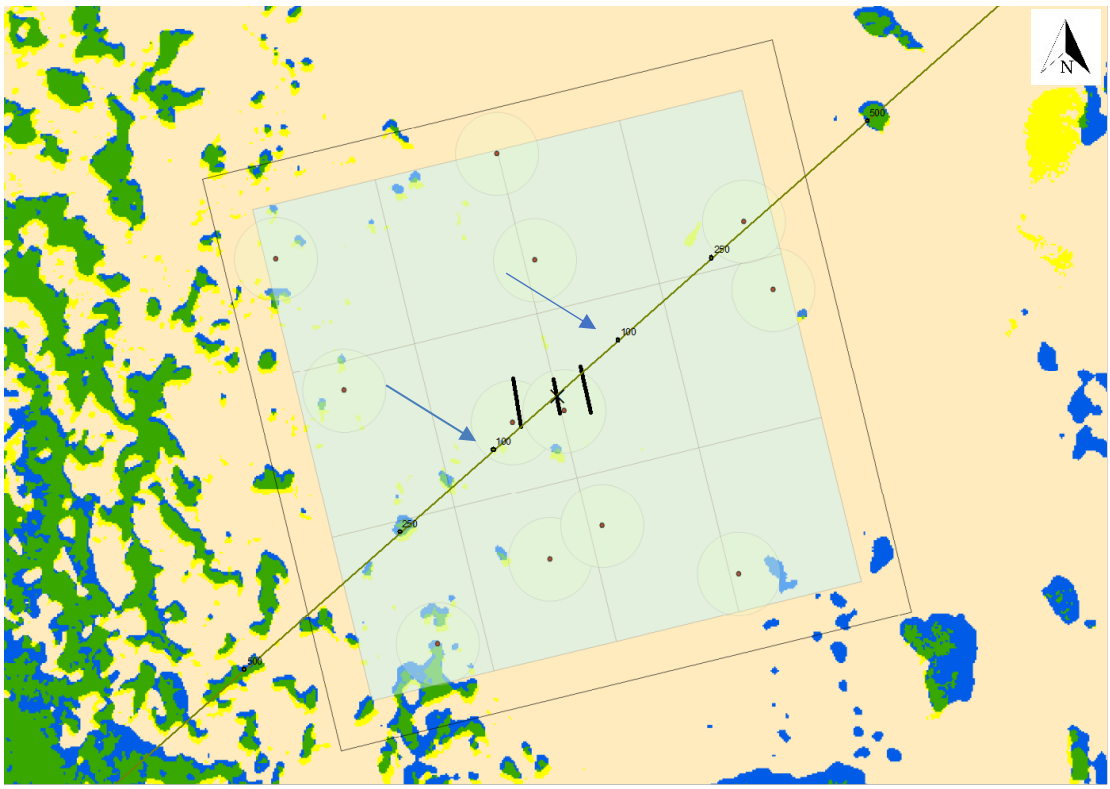

Figure 26: Position of pressure sensors and ADCP in the proximity of the Glenelg shellfish reef (black bars). The two blue arrows point out the location of one pressure sensor (North-East) and the ADCP (South-West), positioned 100 meters from the reef centre (black lines). Picture courtesy of Rob Daly, Senior Scientist-SA Water. Reproduced with permission.

Two Pressure sensors were deployed by SA Water personnel at approximately 1.6 meters from the seafloor, while the ADCP was positioned at 0.25 meters from the seafloor. One pressure sensor and the ADCP were located at the same location, 100 meters South-West from the reef centre (271,511.32E 6,127,043.75N), while a second pressure sensor 100 meters North-East (271,652.60E 6,127,185.03N) from the centre of the reef (blue arrows on Figure 26). The pressure sensors collected the data from the 17th of March 2021, starting at 8:40am, to the 12th of May 2021, at 13:50pm, while the ADCP measured parameters from the 26th of March, at 9:00am to the 16th of April 2021, at 13:00pm.

1.2.1 Pressure sensors

The pressure sensor used for the project was the RBR*solo*^{3}DWave (Figure 27); it provides information on parameters such as significant wave height (*Hs*), peak period (*Tp*), ten percent wave height (*H1/10*) and associated period, maximum wave height (*Hmax*) and associated period, average wave height and associated period. The instrument samples by detecting the average pressure changes in the water column (RBR 2021). The pressure sensor collected information in the Glenelg reef continuously, at a sampling frequency of 16Hz, for two minutes, every ten minutes. Data were then processed and provided by SA Water.

Picture removed due to copyright restrictions.

Original available online: https://rbr-global.com/products/compact-loggers/compact-tide-wave

Figure 27: The picture shows the RBRsolo^{3}DWave used for the project. Source: RBR (2021)

When wave-related parameters are measured, a specific number of data is collected at a specific time, and the operation is repeated for a series of preselected intervals (RBR 2021). Therefore, it is important to configure three main settings before using the instrument, such as speed, duration of the operation (number of data to be collected) and the interval for bursts repetitions (RBR 2021). In addition, for wave measurements, it is essential to specify the altitude at which the instrument is deployed (in meters, above the seafloor) and the mean water depth (RBR 2021), where the instrument is allocated. The wave recorder bursts both continuously and intermittently, and in that way, it can capture even low frequency waves (RBR 2021). The data collected by the RBR pressure sensor are then processed with the Ruskin software, which produces information about waves' compositions (e.g., wave energy) (RBR 2021).

1.2.2 ADCPs

An acoustic Doppler current profile (ADCP) (Figure 28) is a hydroacoustic current meter with a sampling frequency range of 38 kHz to several Megahertz. The ADCP used during the data collection for the Glenelg shellfish reef was mounted 25 centimetres from the seafloor, facing upwards and it measured wave period, wave height and wave direction during a seventeen-minute burst, at 1Hz, every four hours. The data collected were significant wave height (*Hm0*), peak period (*Tp*), mean period (*Tm02*), mean 1/10 height (*H10*), maximum height (*Hmax*) and mean height (*Hmean*). Furthermore, the ADCP provides information on peak direction (*DirTp*), directional spread (*SprTp*) and mean wave direction (*MeanDir*) (Ocean Illumination n.d.). Data for the ADCP were processed using a specific software called Nortek Storm and provided by SA Water personnel.

ADCPs are mostly used for measuring water current velocities on a range of depths, and they use the Doppler effect of sound waves scattered by particles within the water column (Songnian, J. 1992). An ADCP uses four beams to measure wave generated orbital velocities (Ocean Illumination n.d.) and in addition, a fifth beam is used as an altimeter to measure the distance from the surface (Ocean Illumination n.d.).

Picture removed due to copyright restrictions.

Original available online:
https://www.nortekgroup.com/assets/software/N3015-031-ComprehensiveManual_ADCP_1118.pdf

Figure 28: Picture of an ADCP with the four beams. Source: Nortek AS (2018).

ADCPs contain elements called transducers to transmit and receive sound signals. In recent years, more functionalities and components have been added to ADCPs (Wanis and Hull 2011) such as a clock to measure travel time, a temperature sensor, a compass for direction and a rotation sensor for orientation. To make the measurement, the instrument must be submerged with the sensors generally facing downward, although there may be installations where the instrument is fully submerged and placed horizontally, in order to measure the transverse profile of the current (Songnian 1992). ADCPs can also be placed on the sea floor, facing up to measure the velocity and direction of currents, at equal intervals up to the surface. In addition, ADCPs mounted laterally on a wall, pier, and/or piles in rivers or canals can measure the current profile from bank to bank, while in very deep waters they can be attached to cables from the surface (Muste et al. 2002). Wave measurements are generally available for instruments placed on and/or near the seafloor, but recent improvements allow the instrument to also be deployed on rotating buoys, below the surface (Boyd 2006). In addition, it is also possible to estimate wave characteristics during extreme weather events, with appropriately configured ADCPs, through a dissipation rate estimation which is possible from fixed installations, and from mobile underwater structures, such as gliders or underground buoys (Yamashita 1999).

1.3 Numerical Modelling

Numerical modelling was performed to analyse the potential for wave attenuation by the Glenelg Shellfish Reef using the software Delft3D (Figure 29).

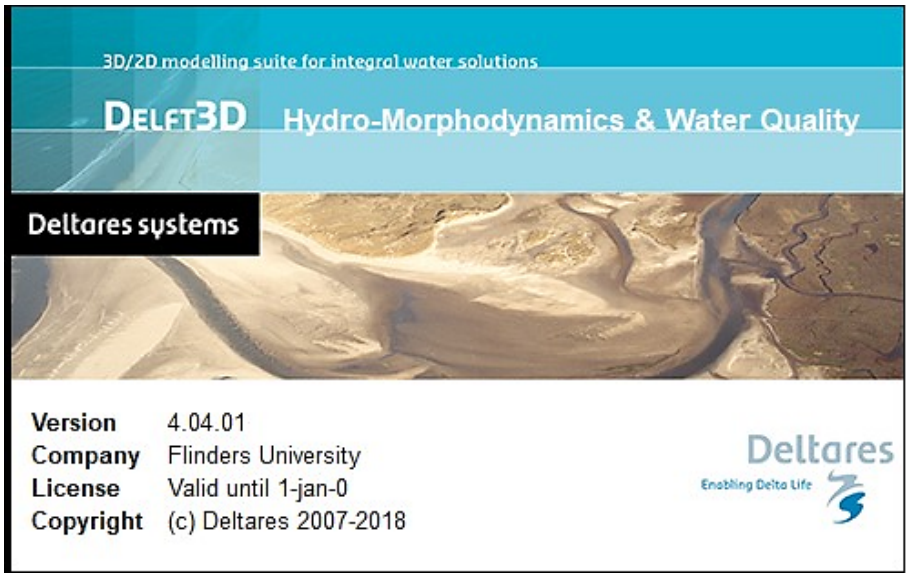

Figure 29: Delft3D software opening interface. The version 4.04.01 has been used for the research project, with the license provided by Flinders University.

The software Delft3D was developed by Deltares, and it is used worldwide for hydrodynamic and morphological simulations in coasts, rivers, lakes, and estuaries. Among the possible uses of the software, there are the study of flows caused by tide, wind, density gradients, the interactions between currents and waves on an irregular bathymetry, the study of the transport of coherent and non-coherent sediments and the study of water quality. Delft3D consists of several modules, each one related to its domain of interest: Grid (Grid and bathymetry), Flow (Hydrodynamics, including morphology), Wave, Water Quality (Far-field water quality) and Part (Particle tracking) (Figure 30). For the development of the Glenelg shellfish reef model, the FLOW and WAVE modules were used; Delft3D WAVE works similarly to the SWAN (Simulating WAves Nearshore) software, which operates based on the action balance equation for spectral waves (Booij et al. 1997). SWAN was projected to simulate wave conditions on shallow waters, and it analyses the refraction/diffraction of wave energy, wave energy dissipation by bottom friction and wind-generated waves (Lowe et al. 2009). The modelling of the Glenelg reef was conducted via a procedure with multiple phases. In detail, the adopted method consisted in developing the grids and the bathymetry files for each of the specific area of interest through the GRID module, followed then by the nesting of the developed grids and the simulation for the FLOW component, without considering the action of waves and/or wind. Waves and wind parameters will be introduced later, with the use of the WAVE module.

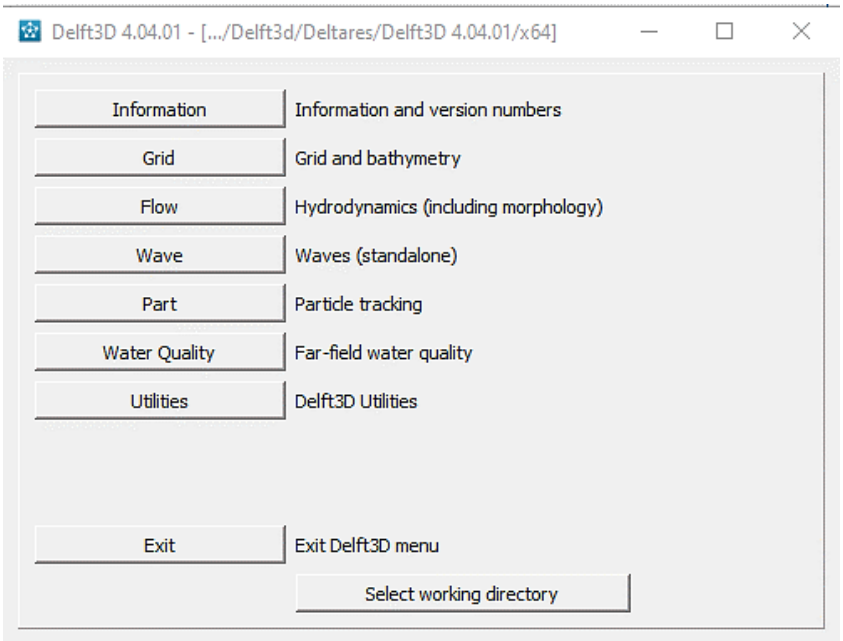

Figure 30. Graphic User Interface (GUI) of Delft3d, with the specific modules.

1.3.1 GRID development

The first step of the Delft3D numerical modelling consisted in the generation of the grid and the specification of its characteristics. The curvilinear GRID (Figure 31) for the coarse domain (Gulf St Vincent) was generated by Deltares, requested by SA Water and it is called AREM (Adelaide Receiving Environment Model). AREM was later provided by SA Water, to Dr Graziela Miot da Silva, College of Science and Engineering at Flinders University, for the Glenelg shellfish reef project.

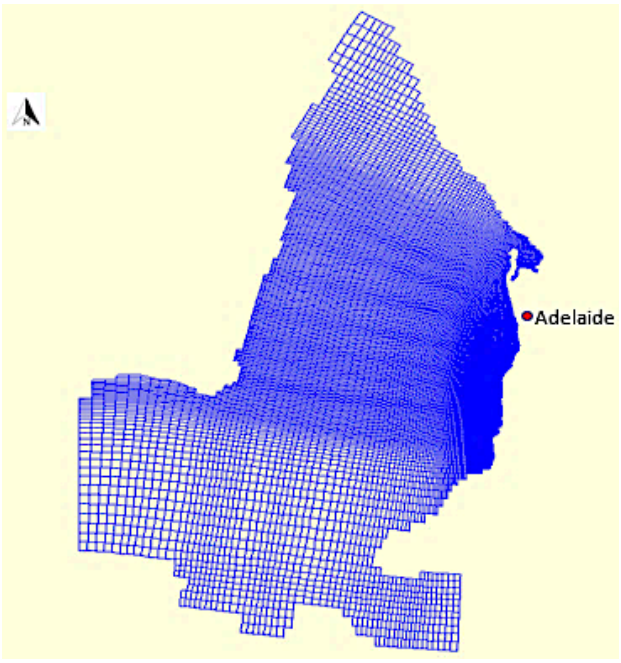

Figure 31: AREM model showing the GRID for the Gulf St Vincent. The GRID becomes finer when it approaches the eastern side of the Gulf, corresponding to Adelaide coastline.

In order to complete the AREM construction phase, the RGFGRID module was used. In particular, the RGFGRID sub-module can be used for the generation and manipulation of the grid, while the QUICKIN module allows to create the bathymetry associated with it. The AREM model consists of a GRID in Cartesian coordinates, with cells that decrease in size as the area of interest is approached, in this case, the coast along the city of Adelaide. The dimensions of the grid, starting from the coarser area of the model are 1226.46 meters in width (N) and 2464.87 meters in length (M), while moving towards the shoreline, AREM becomes finer, with cells of dimensions corresponding to 200 meters in width (N) and 268 meters in length (N), right to the coastline. For details regarding the AREM model development see the report for the Adelaide Receiving Environment Model (Zjil et al. 2014). Starting from the Gulf Saint Vincent grid (AREM model), the objective was to obtain four nested grids; each nested grid was refined four times from the original grid cell size. To do so, the use of RGFGRID component was necessary and as first step, four GRIDs of different size were produced (Figure 32; Figure 33). The four GRIDs obtained are called Nested1, Nested2, Nested3 and Nested4, respectively, from the coarsest to the finest.

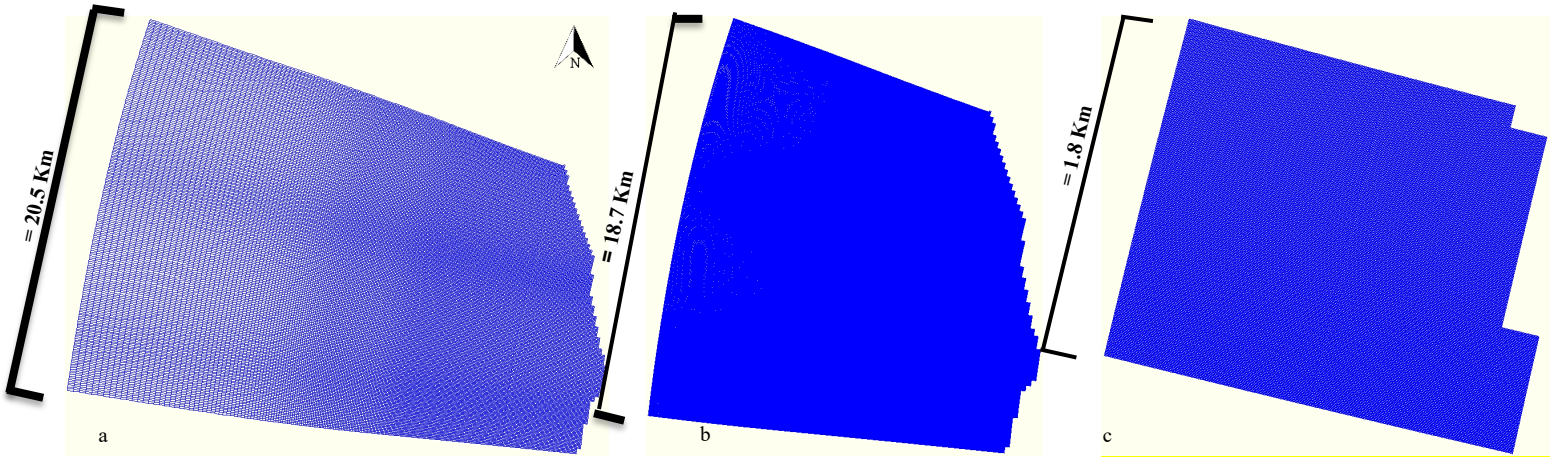

Figure 32: The three GRIDs obtained with the cut and refinement of AREM: (a) Nested1.grd; (b) Nested2.grid; (c) Nested3.grid

Nested1 had cell dimensions corresponding to M (y coordinate) = 60.5 meters and N (x coordinate) = 64.4 meters, Nested2 has cell dimensions corresponding to M= 14.75 meters and N= 22.278 meters and finally Nested3 cell's dimensions are M= 3.81 meters and N= 5.60 meters. The last produced GRID was Nestd4, representing the specific area of the extension of the reef (Figure 38), with cell's dimensions corresponding to M= 1.0 meters and N= 1.0 meters.

1.3.2 Bathymetry Interpolation

The second phase of the project was the interpolation of the bathymetry, consisting in the creation of a continuous surface, starting from point-type data (Amante and Eakins 2016), such as ". xyz" file samples. The interpolation of the bathymetry was used to produce five .dep files, with specific bathymetric characteristics for every developed GRID.

In the case of the AREM model, it was necessary to start with a samples file, ". xyz", in Cartesian coordinates, provided by Geoscience Australia (Australian bathymetry and topography grid, 2009); The samples file for AREM model, was not in UTM coordinates initially, and therefore it needed to be converted to UTM coordinates, using a specific UTM zone (54°) for South Australia. A triangular interpolation was applied to the "xyz" data via QUICKIN and a bathymetry file (.dep) was generated for each large domain (Gulf St Vincent) and the four nested grids. For the triangular interpolation of the bathymetry of the final Nested4, a samples file provided by The Nature Conservancy (TNC) was used, and as visible in Figure 33, the bathymetric characteristics of the Glenelg shellfish reef area and the block of limestones were shown.

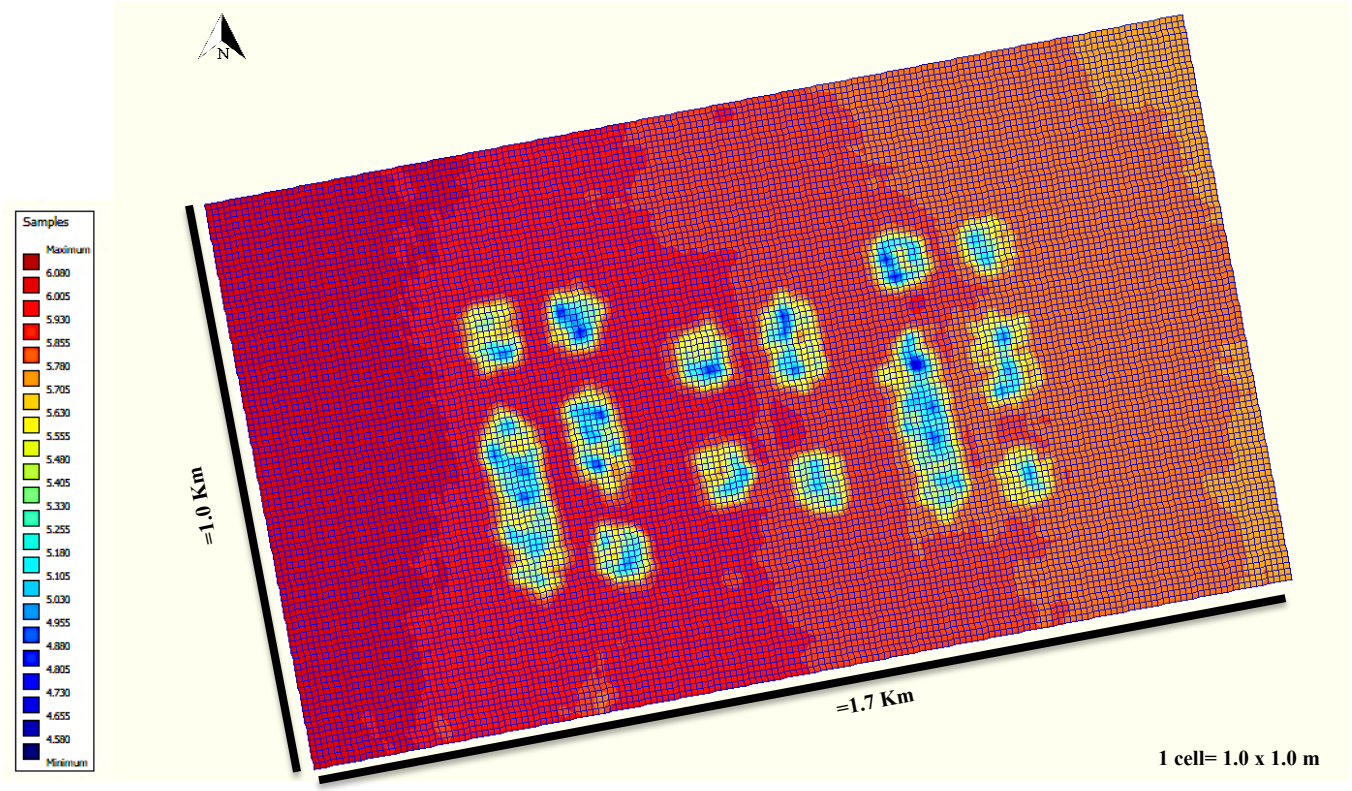

Figure 33: Glenelg shellfish reef bathymetry. The limestone blocks are displayed as individual structures, and their crests range from 4.5 meters to 5 meters, above the seafloor, as visible from the blue/light blue coloured patches. *Source: Courtesy of The Nature Conservancy (TNC)*. Reproduced with permission.

1.3.3 Nesting

Following the generation of the four refined GRIDs, and bathymetry files, other input files were produced for each one of the Nested GRIDS, necessary to start the FLOW simulation, such as the enclosure file (.enc), and the boundary conditions (.bnd). The enclosure file indicates the active grid cells in the domain and at the same time, it delineates the position of the open and closed boundaries (Deltares, 2021). The file with the boundary conditions (.bnd) is the input that defines the type and location of the open boundaries. The boundary file is represented by several sections, each one with a specific name based on its orientation, starting, and ending points and the type of boundary forcing. The boundary conditions consider the different types of hydrodynamic forcing of the flow, such as water level, currents and water levels gradients and those

hydrodynamic factors can be described as harmonic, astronomic, or time-series conditions (Deltares, 2021). There can be several types of boundary conditions available, such as Water level, Velocity, Neumann, Discharge or flux and Riemann (Deltares 2021). For the FLOW simulation, the boundary conditions were kept in water level, for the West boundary of Nested1, Nested2 and Nested3 and the Northwest boundary of Nested4, and in Neumann for the remaining boundary conditions (North, South, Southwest, Northeast and Southeast) of the four Nested GRIDs. The type of boundary specified in Neumann allows to have a water level gradient along the coast and consequently, it provides greater flexibility to the model, when approaching shallow waters. In that way, computational errors related to water velocity changes too high can be prevented, in shallow waters near the shoreline. As for the outer model, AREM, enclosure file, boundary conditions, and astronomical boundary conditions (.bca file, which reports data related to tidal conditions) were already available from the database provided by SA Water. After the generation of input files, the used method involved Delft3D components NESTING (1) and NESTING (2). Those operations are used to nest one grid with finer resolution within another coarser grid. It is therefore possible to obtain a single grid from multiple GRIDs, with cells of different sizes which will be nested in a precise and specific area; the coarser grid will provide boundary conditions for the nested grid. The completion of the NESTING was performed with the use of OpenEarth Tools (OET) in MATLAB. Open Earth Tools is an open-source solution, for storing and using data, models, and tools important in marine/coastal science and engineering projects (Deltares 2016).

The first nesting phase consisted in the use of the NESTING (1) tool. This tool generates the administration file (.adm) and a file reporting the location of observation stations (.obs), within a defined area in the model. The administration file provides the boundary conditions at the monitoring stations defined by the ". obs" file, while the observation file lists monitoring stations the nested models (Deltares 2021). It can be graphically observed in Figure 34, (A) and (B) how the different GRIDs appear after the NESTING (1) phase, using the RGFGRID component of the software.

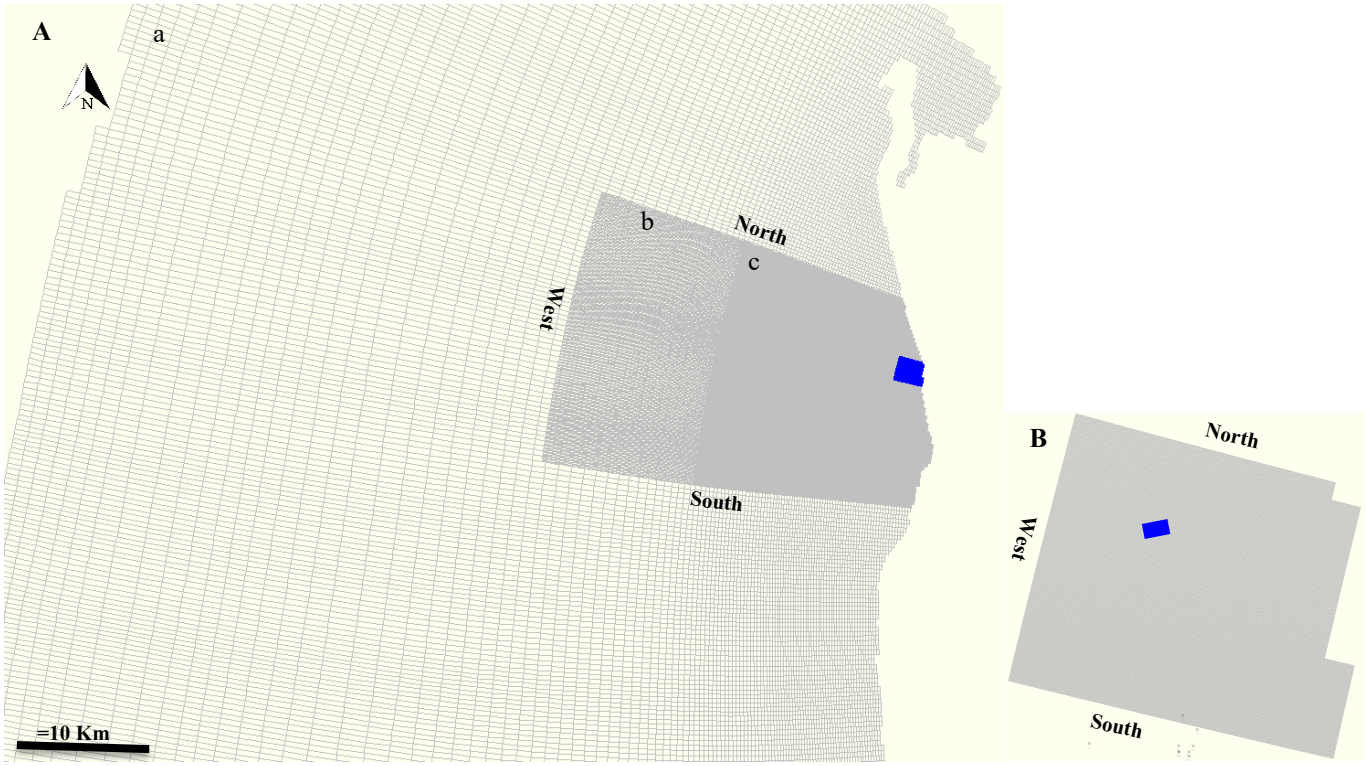

Fig 34: (A) The outer GRID AREM and the three nested Inner GRIDs: (b) Nested1, (c) Nested2 and the blue rectangle representing Nested3; (B) For graphic reasons the final nesting with Nested4 corresponding to the blue rectangle in Nested3 is provided separately. In the picture, the names of boundary conditions are also indicated.

Once the NESTING (1) phase was completed, two important steps followed: a FLOW simulation was started for AREM to to obtain output files, called history files necessary for the following nesting phase in OET, NESTING (2). Through NESTING(2), time-series flow boundary conditions files (.bct) were created for Nested1. Those two phases, FLOW simulation and generation of a .bct file were repeated for each one of the Nested GRIDs to obtain four specific time-series flow boundary conditions.

1.3.4 Delft3D-FLOW

The hydrodynamic module Delft3D FLOW provides simulations of flows, resulting from tidal or meteorological forces on curvilinear or rectilinear grids. The flow model (.mdf) can be generated in the Delft3D graphical user interface, from input files, and the obtained results are then displayed through QUICKPLOT. The FLOW computation was carried out for a specific timeframe, from the 27th of August 2021 at 00:00 am, until the 29th of August 2021, at 00:00am. Simulations have been performed for each one of the GRIDs, starting from AREM, up to Nested4 model, using for each one of the models, the monitoring stations obtained from the NESTING (1), of the previous model (e.g., Nested1.obs used for AREM FLOW computation). The interval chosen for every computation was 60 minutes, while the number of time-steps per second varied to avoid errors, related to too high-water velocity changes. For AREM, Nested1, Nested2 the simulation foresaw one time step every minute, while for Nested3 and Nested4, the model considered 1 timestep every 0.1 seconds. Table 2 provides information on the physical parameters used for the FLOW simulation.

Constants	**Roughness**		**Viscosity**
Gravity	**Bottom Roughness**		**Horizontal eddy viscosity**
9.81 m/s^2	**Roughness Formula**	**Value**	1 m^2/s
	Chezy	Uniform (U=65; V=65)	
Water density	**Wall roughness**		
1000 Kg/m^3	Slip condition Free		

Table 2: Physical parameters for Nested4 Flow simulation in Delft3D. The model physical parameters were kept at default settings.

Delft3D-Flow used the equation below to calculate the bed shear stress ($\vec{\tau}_c$) in N/m^2.

$$\vec{\tau}_c = \frac{g\rho 0\vec{U}\left|\vec{U}\right|}{C_{2D}^2}$$

Where:

g= acceleration due to gravity (m/s^2)

ρ= water density (kg/m^3)

$\vec{U}$= magnitude of depth-averaged horizontal water velocity (m/s)

C_{2D}^2= Chézy coefficient

1.3.5 Delft3D WAVE

The second type of simulation carried out for the project was a specific WAVE model for Nested4.
The module Delft3D WAVE simulates the evolution of wind-driven waves within the model domain. It is possible to calculate wave propagation, wave generation due to winds and wave-wave interaction. The WAVE component works similarly to FLOW: WAVE inputs can be defined; a computation can be started through the START sub-module and the results can be evaluated with the use of QUICKPLOT. The WAVE

model for Nested4 was developed based on a wavecon file which contains the time-series of wave conditions the wave conditions, to be used during the simulation. The wavecon file is automatically recognized by the WAVE module at the time of computation, if placed in the working directory. A series of parameters have been specified in the wavecon file such as the significant wave height in meters (*Hm0*), the peak period (*Tp*) of the energy of each wave expressed in seconds, the mean wave direction (*MeanDir*) expressed in degrees and the width energy distribution, representing the standard deviation expressed in m s^{-1} or in degrees and the water level for the specific time-points.

Wind speed and wind direction were kept at 0. The data collected by ADCPs for *Hm0*, *Tp* and *MeanDir* inserted in the wavecon file were provided by SA Water, with a starting time on the 26th of March 2021, at 9:00am, and data measured every four hours, until the 16th of April 2021 at 13:00pm. Table 3 indicates the conditions for the physical parameters used for Nested4 Wave simulation.

Constants	**Wind**		**Processes**		**Various**
Gravity	**Uniform Wind**		**Generation mode for physics**		**Processes activated**
9.81 m/s^2	**Speed**	**Direction**	3-rd generation		Whitecapping (Komen et al.)
	0 m/s	0°			**Wave propagation in spectral space**
Water density					Refraction
1000 Kg/m^3					Frequenty shift
North w.r.t. x-axis			**Depth-induced breaking (B&J model)**		
90°			**Alpha**	**Gamma**	
Minimum depth			1	0.73	
0.05 m			**Bottom friction**		
Convention			**Type**	**Coefficient**	
nautical			JONSWAP	0.067 m^2 s^{-3}	
Forces			**Diffraction**		
wave energy dissipation rate 3D			none		
Wave-set up					
none					

Table 3: Physical parameters for Nested4 Wave simulation on Delft3D. The model physical parameters were kept at default settings.

The equation below is used by Delft3D-Wave to calculate the orbital velocity near the bed (u_{orb}), measured in m/s and based on the linear wave theory (Krogstad and Arntsen 2000), given by:

$$u_{orb} = \frac{1}{4}\sqrt{\pi}\frac{H_{\mathrm{rms}}\,\omega}{\sinh\,(kH)}$$

Where:

H_{rms}= root-mean-square wave height

ω = angular frequency waves (1/s)

k = turbulent kinetic energy (m^2/s^2)

H= total water depth (m)

1.3.6. Model Validation

The model was validated by exporting data for the significant wave height, by selecting a specific point in the North-East area of Nested4, with coordinates corresponding to 271, 652.60E; 6.127.155N. The coordinates were chosen according to the position (271,652.60E; 6,127,185.035N) of the North-East pressure sensor deployed by SA Water, in order to compare the field data for the significant wave height, with data exported from Delft3D. Subsequently, for the visualization of the trend, two graphs have been made using Office Excel, to detect the trend of the significant wave height and potential similarities and/or variations between the field data and the model. To evaluate the accuracy of the model, the Root Mean Square Error (RMSE) (Equation 1) was as well calculated, where:

$$RMSE = \sqrt{\sum_{i=1}^{n} \frac{(\hat{y}_i - y_i)^2}{n}}$$

$\hat{y}_i$ = predicted value

y_i = observed value

n = number of observations

Furthermore, the coefficient of determination R^2 was used to analyse the differences among the two variables, Field data and Model data, more specifically, it evaluates the correlation between every datapoint of the two data pools.

RESULTS

With the use of Delft3D Flow and Wave modules, the simulation of specific hydrodynamic conditions for the Glenelg shellfish reef was computed. The following results present an analysis of the main parameters observed.

1. Model Validation

Figure 35 shows the comparison of the significant wave height variation trend of the simulation, with the data collected by the Northeast pressure sensor, located 271,652.60E and 6,127,185.03N (Figure 26). For the purpose of the validation, both the model data and the field data were daily averaged. Overall, the wave model is able to correctly simulate the trend of the measured significant wave height, but it overestimates the wave height, especially during days of higher significant wave height *Hm0* (e.g., 9th-11th of April 2021 and 13th-15th of April 2021).

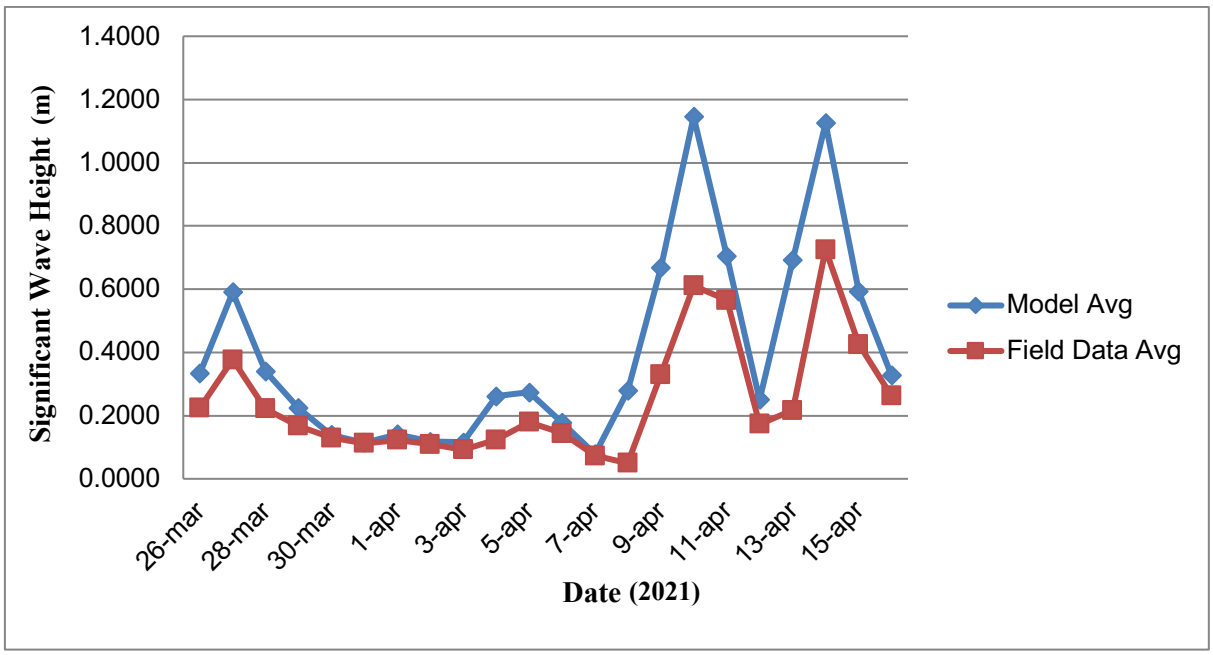

Figure 35: The graph shows the comparison in the trend for the averaged significant wave height for the Wave model and the Field data, from the 26th of March 2021 to the 15th of April 2021.

In order to measure the accuracy of the model, the RMSE (Root Mean Square Error) has been calculated, corresponding to 0.2134; the lower the RMSE, the higher the model accuracy, and in this case, the value indicates a good predictive model. Furthermore, based on the scatter graph in Figure 36, and the calculation of the coefficient of linear regression (R^2), it is possible to observe the correlation between the two variables analysed. R^2= 0.8574 indicates a positive correlation between the two variables, with the 85% of the points corresponding to the regression line.

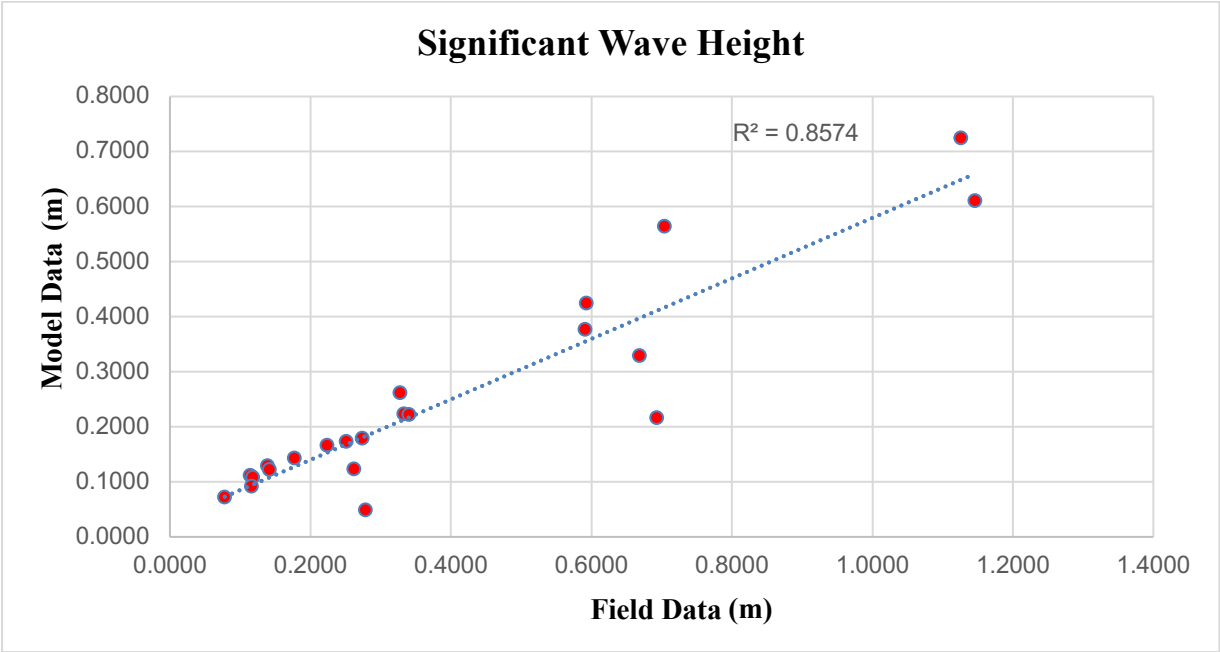

Figure 36: Scatter plot, with the R^2, indicating a positive correlation between the two variables, Model data and Field data.

2. Flow Model

2.1 Water Level

Figure 37 (A) and (B) shows a decrease in water level in the Glenelg reef area, corresponding to the incoming peak of low tide on August the 28th, 2021, at 13:09pm (Bureau of Meteorology, 2021). It is possible to notice the direction of the flow seaward, from the shoreline (East) towards offshore (West), and at the same time, a minimal progressive decrease of the water level towards the offshore, corresponding to 0.59 centimetres, from 09:00am to 10:00am. It is possible to observed in the figures, particularly in Figure 37 (A), the influence of the reef's boulders.

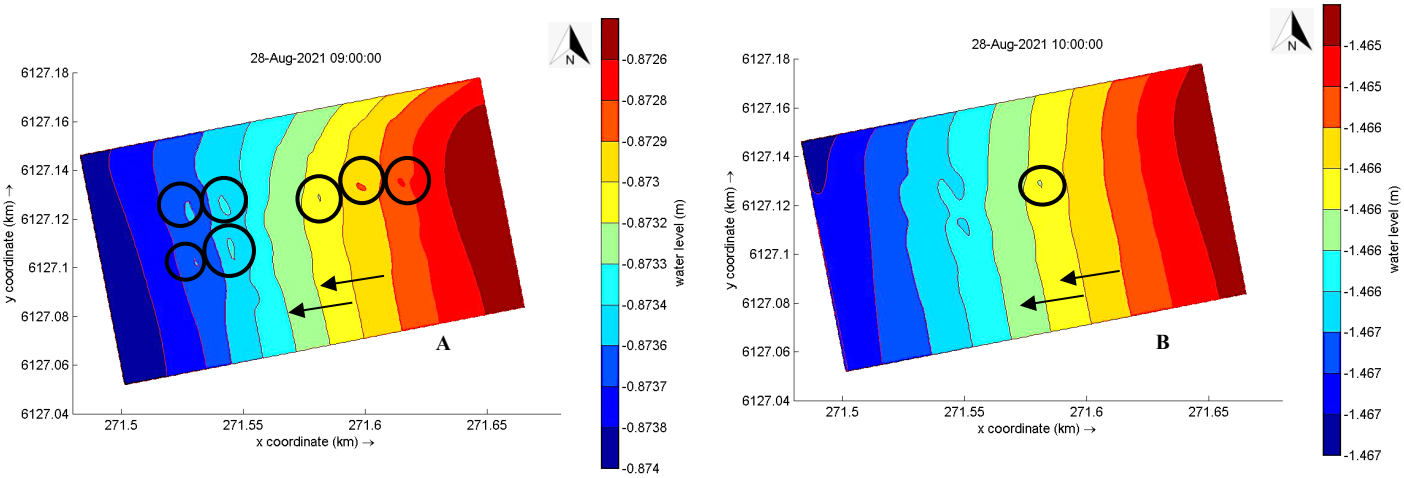

Fig 37: (A) 28th of August 2021, at 9:00am; (B) 28th of August 2021, at 10:00am. The Figure indicates the tidal flow moving from the shoreline to offshore and a progressive decreasing in the water level, with the incoming low tide. The black circles point out the reef's boulders. The black arrows indicate the outgoing tidal flow direction.

With the high tide (2.2 meters) approaching for the 28th of August 2021, occurring at 19:00pm (Bureau of Meteorology, 2021), it can be observed in Figures 38 (A) and (B), an incoming tidal flow from offshore (West) to the shoreline (East) and simultaneously, an increasing water level. The water level increases about 25.6 centimetres from 16:00pm to 17:00pm (Figure 38).

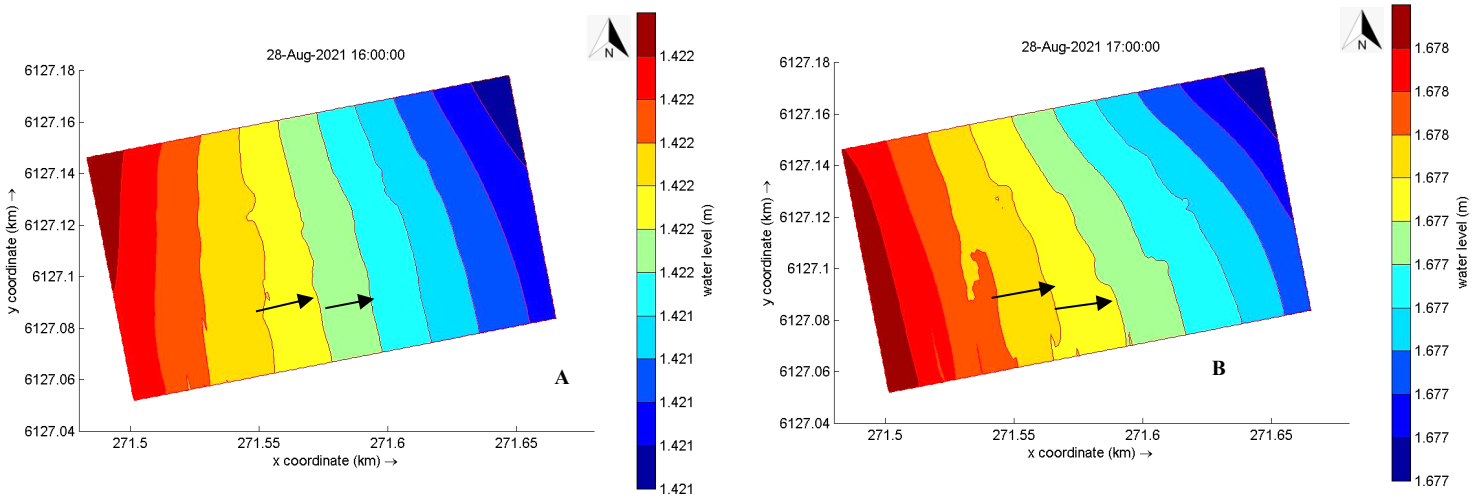

Figure 38 (A) and (B): the Figure shows the increasing water level, from offshore to the shoreline, corresponding to the incoming high tide.

2.2 Bed shear stress

Figure 39 below shows the progressive decreasing of the bed shear stress towards the Northwest. It can be observed how there is a variation when the flow encounters the resistance created by the different reef's structures, compared to the area within the reef, where the bed shear stress decreases. On the reef's boulders the bed shear stress reaches a value of 0.008 N/m^2, while within the reef, it can be observed how it decreases to around 0.004 N/m^2. The difference is minimal, but present and can be quantifiable in an increase of the bed shear stress of the 50% on the crests of the reef 'structures.

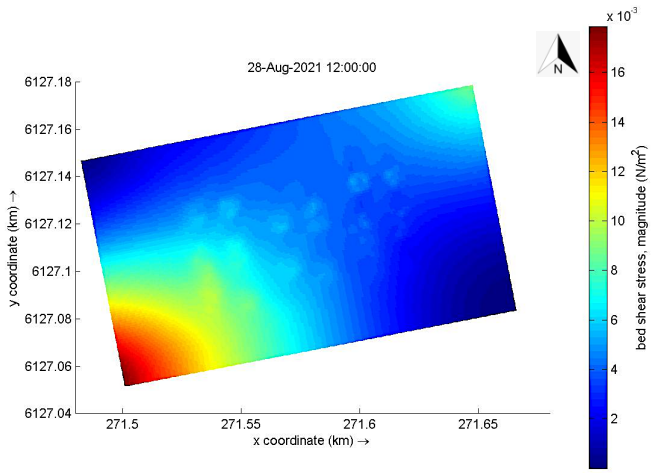

Figure 39: Bed shear stress. It can be observed a mild increasing on the crests of the reef's boulders (light blue) compared to the zones within the structures (blue).

3. Wave Model

Three main parameters were analysed with the Wave model: significant wave height, wave energy dissipation and orbital velocity. Two types of definitions will be used for the sampled days, such as "*calm*" and "*storm*" days, according to the variation of the significant wave height (Hm0). The variation of significant wave height observed for the sampling period is shown in Figure 40. Two higher peaks can be observed in the graph (Figure 40), which correspond to two storm events, occurred on 9th -11th of April 2021 and 14th -15th of April 2021.

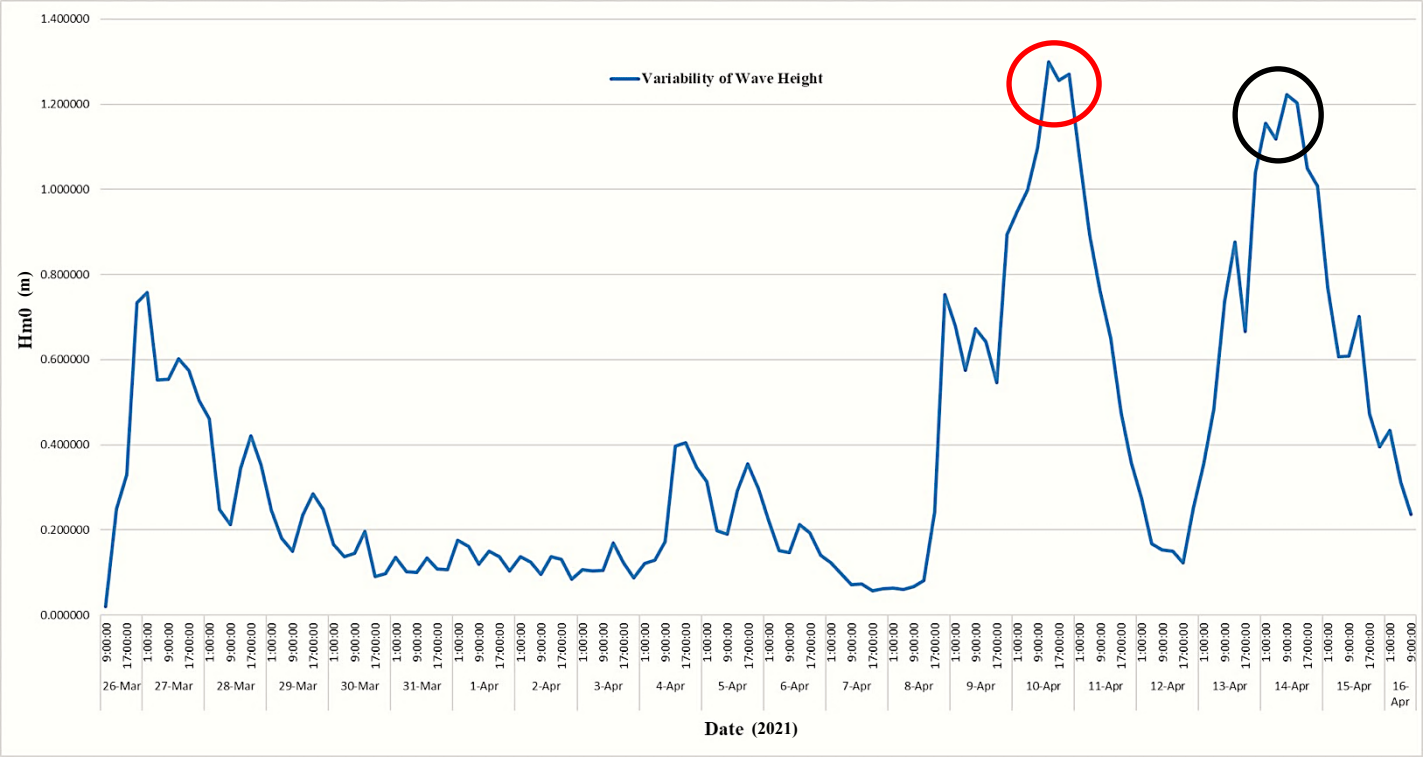

Figure 40: Variability of Wave Height. The two highest peaks on the graph indicates two storm events, starting from the 9th of April 2021 to the 11th of April 2021 (red circle) and from the 14th of April 2021 to the 15th of April 2021 (**black circle**).

3.1 Significant Wave Height

Significant Wave Height (m)		
Sampling Period	**Hm0**	**Condition**
27/03/2021, 05:00am	0.84 m	*calm*
10/04/2021, 17:00pm	1.28 m	*storm*
14/04/2021, 9:00am	1.12 m	*storm*

Table 4: The table shows characteristics of the three samples days, used to represent the model's results related to the variation of significant wave height (*Hm0*). They are referred to as "*calm* "or "*storm*" based on *Hm0* values.

Figure 41 shows significant wave height in meters and wave direction simulations, for the 27th of March 2021, at 5:00am (Table 4). It is possible to observe a gradual reduction of the significant wave height across the reef.

The model measured incoming waves, with a significant wave height of 0.55 meters at the entrance of the reef, a minimum value of 0.53 meters within and outside the reef and a highest 0.57 meters, on the crests of the boulders (Figure 41). Furthermore, the significant wave height is reduced within the reef's structures, gradually from the entrance of the reef (West), and it appears to continue mostly towards North. The significant wave height decreases by the 4%, from the entrance of the reef to its inner zones, while it decreases by a total of 7.5%, from its crests to the inner and exit zones.

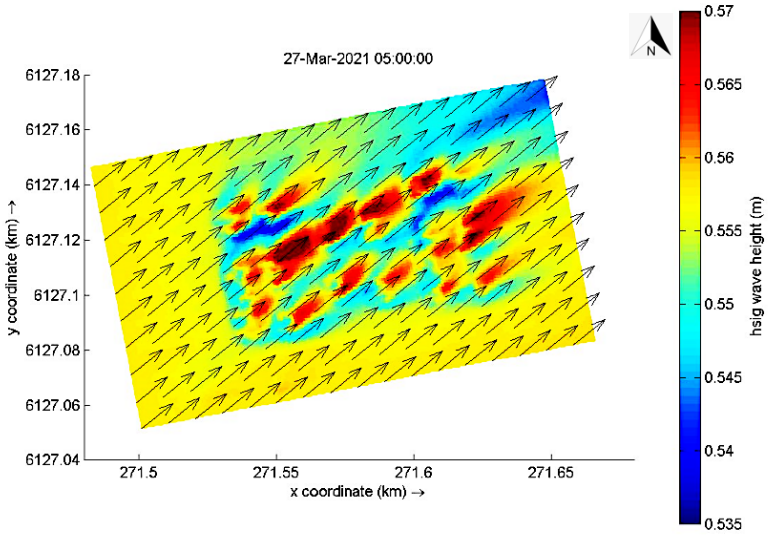

Figure 41: The picture shows the wave direction for the 27th of March 2021, at 05:00am. It can be observed how the waves are coming from Southwest towards Northeast, with a consequent decrease in the significant wave height in the North-eastern area outside the reef.

In Figure 42, it is as well observed the wave direction, with most waves coming from Southwest, in both "*calm*" and "*storm*" days.

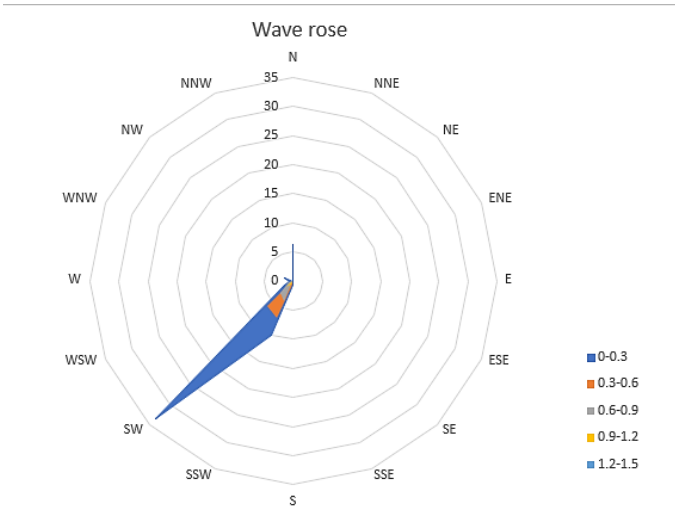

Figure 42: Wave rose showing the directions of waves for the sampling period 26th of March 2021- 16th of April 2021. It is observed how the waves are mostly coming from Southwest, towards Northeast.

On the 10th of April, at 17:00pm and the 14th of April 2021, at 09:00am (Table 4), the wave model results indicate a reduction of the significant wave height, from a maximum of 1.35 meters (red), to a minimum of 1.15 meters (light blue) (Figure 43), corresponding to a minimal decrease of 15%. It can be also observed, how the highest significant wave height mildly increases (few centimetres), over the crests of the reef boulders and when waves exit the reef.

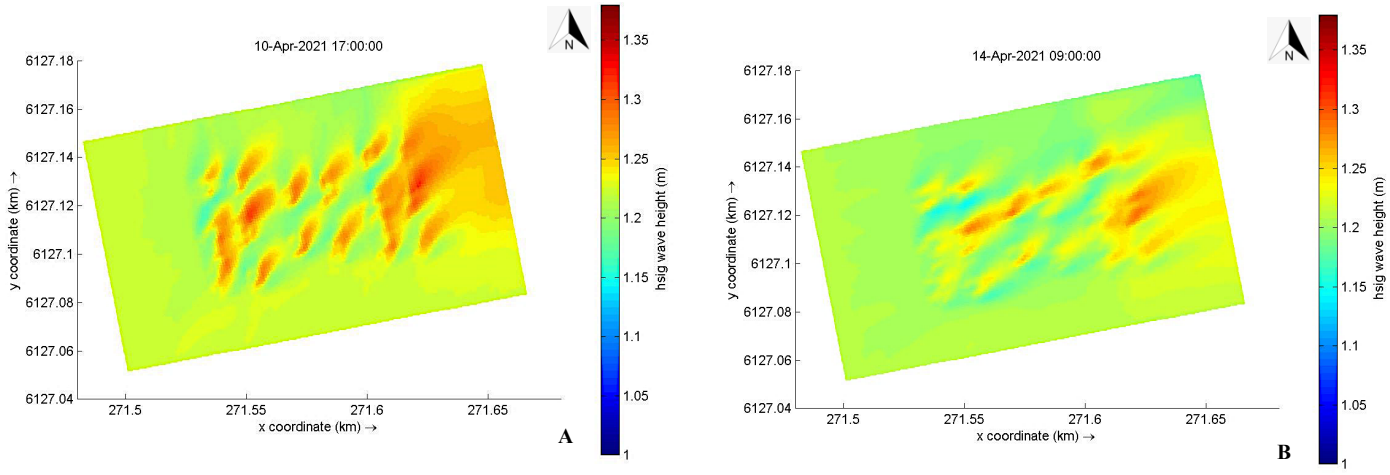

Figure 43: Frames of the Delft3D Wave simulation. (A) 10th of April 2021 at 17:00pm; (B) 14th of April 2021, at 9:00am. It is possible to observe in detail, the reduction of the significant wave height (light blue), at the centre of the reef that continues North (A) and North-East (B).

The Figure (44) below shows the two grid points with coordinates 271,510.2 E 2,6127,067 N (Southwest) and 271,634.9E and 9,6127,163N (Northeast) used to interpolate significant wave height data in the plot, in Figure 50. The two different grid points were selected based on the location of the pressure sensor (Northeast), recording the input data (Field data) used for the model validation, and the location of the ADCP (Southwest), representing the output data (Model data).

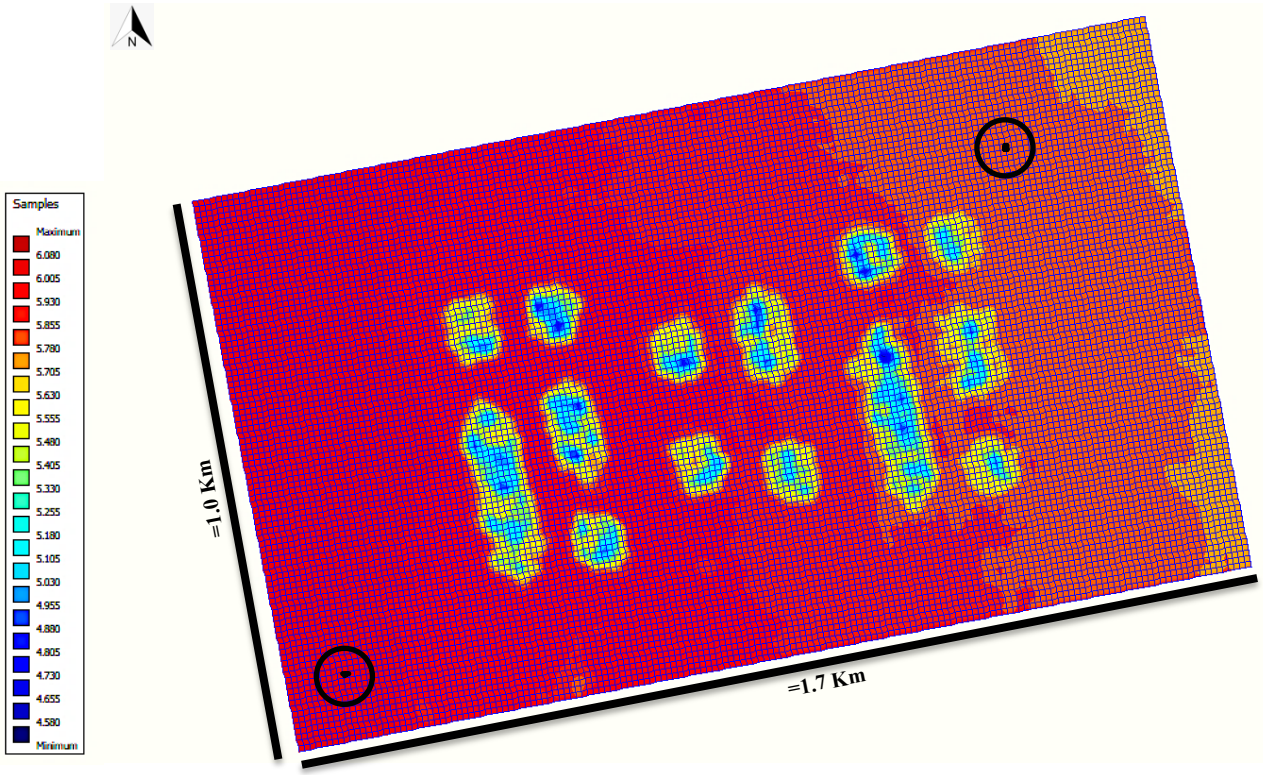

Figure 44: Two grid points (**black dots** circled in white) used for exporting the data on significant wave height, to compare the variation between the Southwest and the Northeast areas of the reef. The data exported from Delft3D for the two location points were used to compare the variation in *Hm0*, between Southwest and Northeast, as visible in Figure 45.

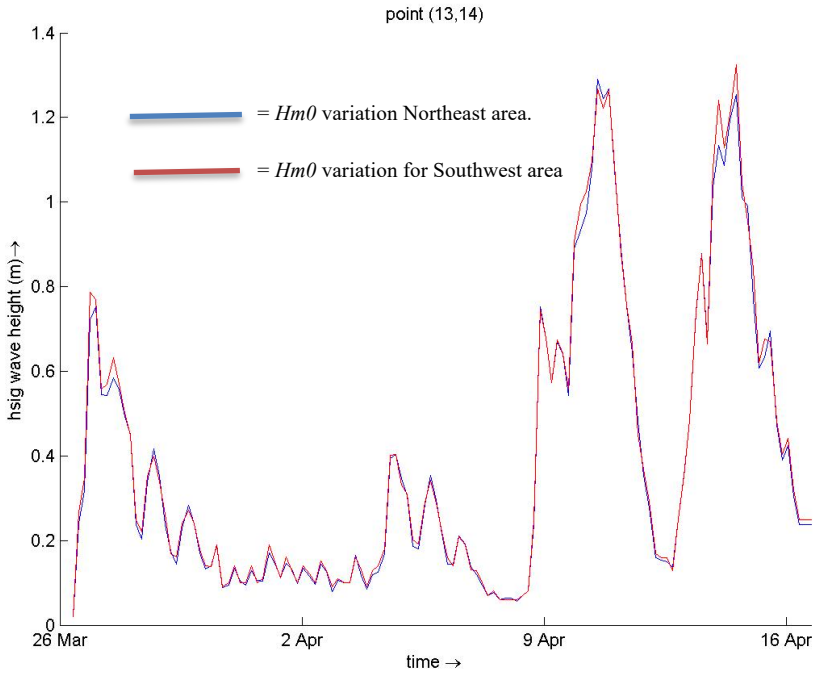

Figure 45: The picture shows the trend for the changes in significant wave height. The red line shows the trend of the *Hm0* for the Southwest area of the reef, while the blue line represents the variation of significant wave height in the Northeast zone. It can be observed how there is a minimal difference between Southeast and Northeast, with the significant wave height decreasing in the Northeast area.

3.2 Dissipation

Wave Energy Dissipation		
Sampling Period	**Hm0**	**Condition**
29/03/2021, 05:00am	0.28 m	*calm*
29/03/2021, 09:00am	0.18 m	*calm*
10/04/2021, 17:00pm	1.28 m	*storm*

Table 5: The table shows characteristics of the three samples days, used to represent the model's results for the variation of the wave energy dissipation. They are referred to as "*calm* "or "*storm*" based on the value of the significant wave height (*Hm0*).

The use of Delft3D Wave module was used to observe changes in wave energy dissipation within the reef. Dissipation is provided in N (Newton) m^{-1} s^{-1}. In the following results, the 29th of March 2021 is showed because of its particularly low values of significant wave height (Table 5). The increase in the wave energy dissipation is especially evident in the proximity and directly on the crests of the reef's structures (red), where the water level is lower, and the waters are shallower. It is important to highlight, that for the 29th of March 2021, at 5:00am (Table 5), the dissipation of wave energy continues when waves exit the reef (Figure 46 (A)); The amount of wave energy dissipation, in Figure 46 (A) highlights how it reaches 0.025 N m^{-1} s^{-1} on the crests of the reef's structures. At 9:00am (Table 5), the highest wave energy dissipation corresponds to 0.02 N m^{-1} s^{-1} (Figure 46 (B)); it mildly decreases (25%) and that is related to the slight increase of the water level from -0.61 meters (05:00am) to -0.27 meters (09:00am).

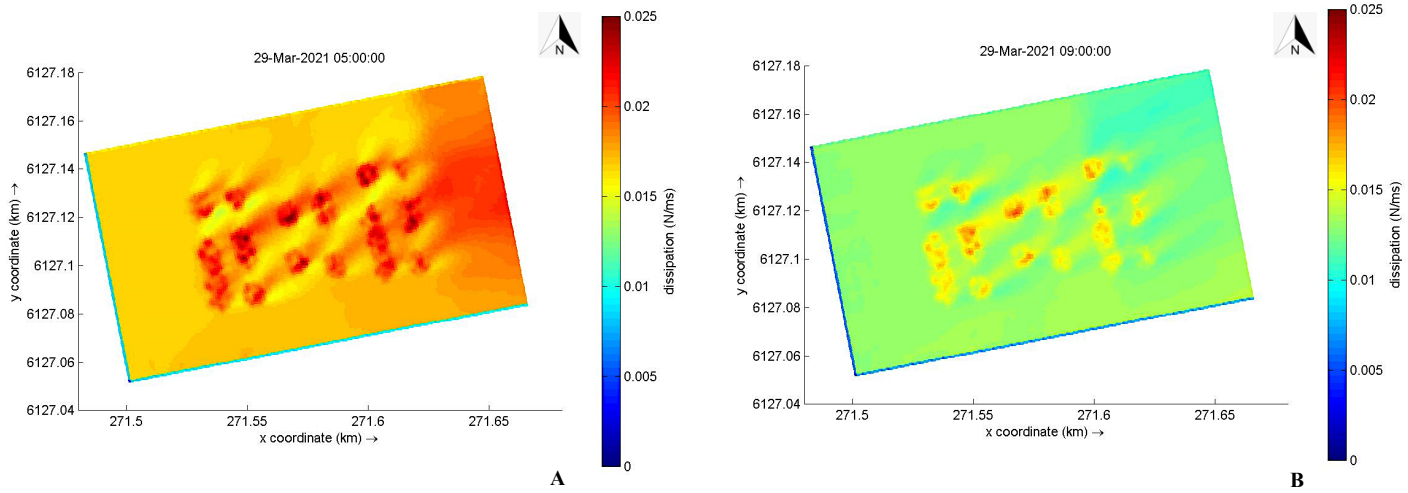

Figure 46: Wave energy dissipation. (A) the 29th of March, 05:00am; (B) the 29th of March, 09:00am. The picture shows the magnitude of dissipation with different coloured shades, from light blue, to red, where red indicates the maximum value of dissipated energy, for that specific time.

Figure 47 below shows wave energy dissipation for the 10th of April 2021, at 17:00pm (Table 5). It is possible to observe an increase in wave energy dissipation from the western side to the crests of the reef's

structures, in the proximity of the reef blocks (Figure 47) and it continues towards East. The difference between wave energy dissipated with higher significant wave heights and lower *Hm0*, corresponds to the 36% more energy dissipated with higher waves.

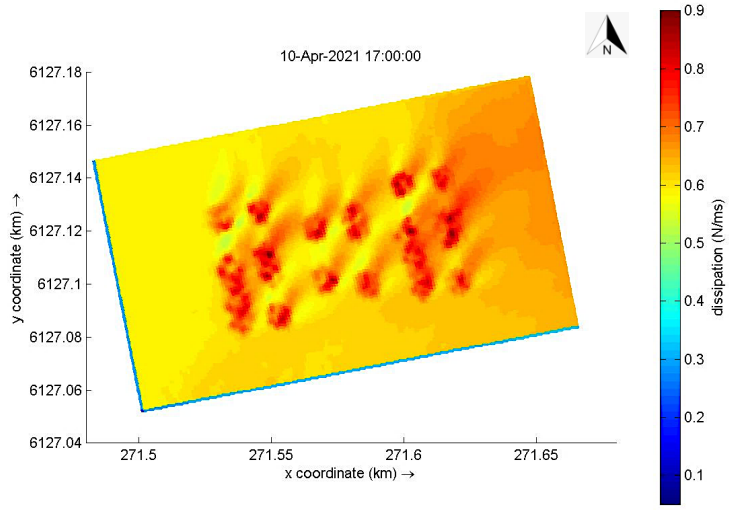

Figure 47: Wave energy dissipation for the 10th of April 2021, at 17:00pm. Wave energy dissipation is mostly on the structures' crests and in the immediate proximity of the reef blocks (red/orange-coloured patches).

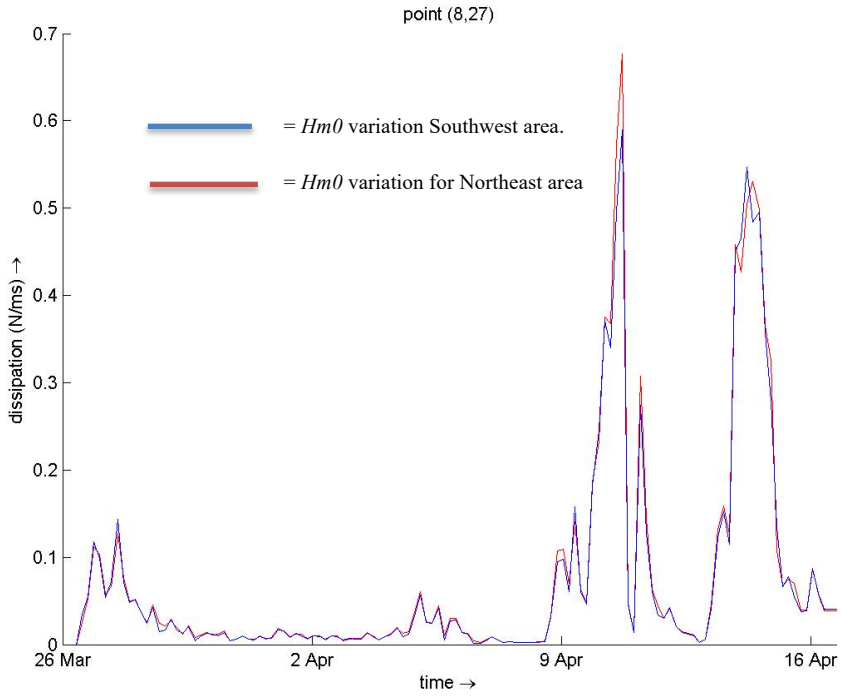

Figure 48: Trend for the wave energy dissipation. The red line shows the wave energy dissipation in the Northeast area of the reef, while the blue line represents the wave energy dissipation plot for the Southwest area of the reef. The plot shows a minimal difference in wave energy dissipation between the two areas, with an increased value for the Northeast of the reef, especially during the two "*storm"* periods.

3.3 Orbital velocity

In DELFT3D Wave module, the orbital velocity near bottom is calculated as the value corresponding to the root mean-square of the maximum of the orbital velocity near the bottom, expressed in m/s (Deltares, 2014).

Wave Energy Dissipation		
Sampling Period	**Hm0**	**Condition**
28/03/2021, 05:00am	0.50 m	*calm*
05/04/2021, 13:00pm	0.16 m	*calm*
10/04/2021, 05:00am	0.98 m	*storm*
14/04/2021, 09:00am	1.12 m	*storm*

Table 6: The table shows characteristics of the four samples days, used to represent the model's results for the variation of the orbital velocity near bottom. They are referred to as "*calm* "or "*storm*" based on the value of the significant wave height (*Hm0*).

Figure (49) below shows the trend of the orbital velocity near the bottom. It is possible to observe a common trend for the 28th of March 2021, and the 5th of April 2021 (Table 6). There is a reduction in the water particles orbital velocity at the bottom, and therefore a decrease in the ability of waves to generate currents near the seafloor, in the central area of the reef, between the different structures of limestone. The magnitude of the orbital velocity in the reef internal areas ranges between 0.13 m/s and 0.15 m/s, while there is an increase in the orbital velocity, on the crests of the reef 's boulders and in the adjacent zones, with values ranging between 0.16 m/s and 0.20 m/s. The total attenuation of the orbital velocity for the reef is present but minimal, corresponding to the 2%. On the other hand, the orbital velocity increases in the areas immediately adjacent to and at the crests of the reef's structures and that indicates a decreasing in the water level, caused by the reef's presence and, consequently shallower waters.

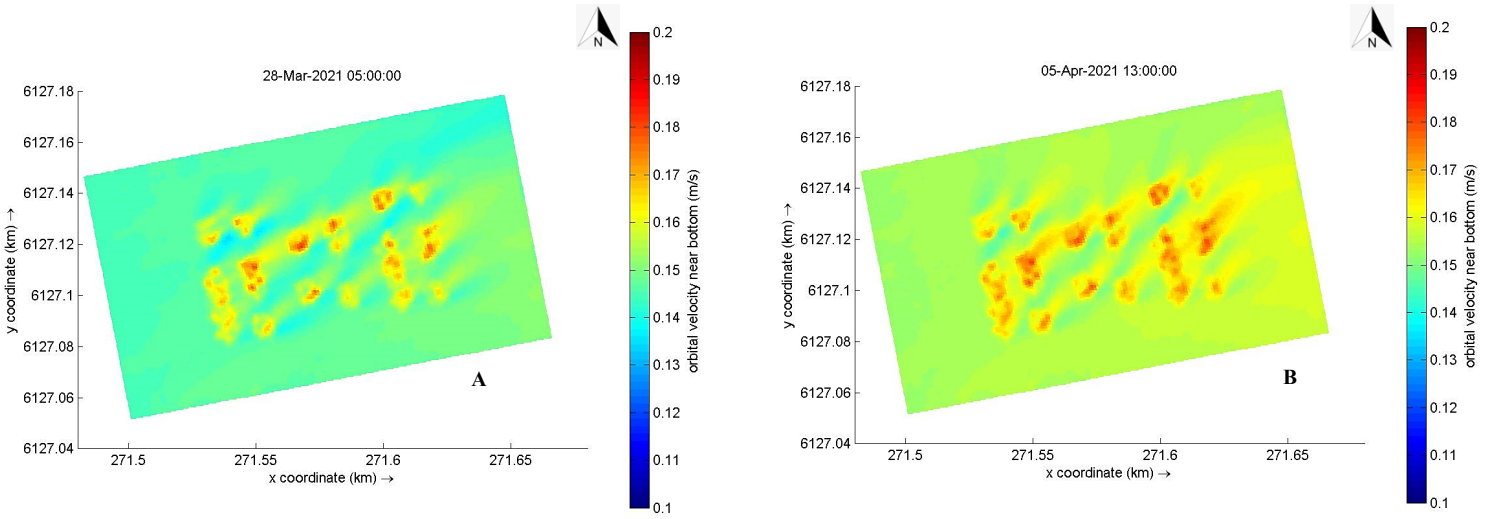

Fig 49: Orbital velocity near bottom. (A) the 28th of March 2021, at 5:00am; (B) 05th of April 2021, at 13:00pm. It can be seen how it decreases in the central area of the reef, while it increases on the top of the reef's structures. The magnitude of the orbital velocity variation can be seen from the colored shades in the picture, where blue is the lowest orbital velocity near the bottom, while the red patches represent the highest value.

For the 10th of April 2021, at 05:00am and the 14th of April 2021, at 9:00am respectively (Table 6), it is possible to observe an increase in the total magnitude of the orbital velocity at the bottom (Figure 50 (A) and (B)), ranging from a minimum of 0.3 m/s to a maximum of 0.55 m/s. In that case, there is a reduction of the orbital velocity in the central area of the reef, corresponding to the 22%. At the same time, the maximum increase in orbital velocity is visible near the individual reef's structures and on their crests.

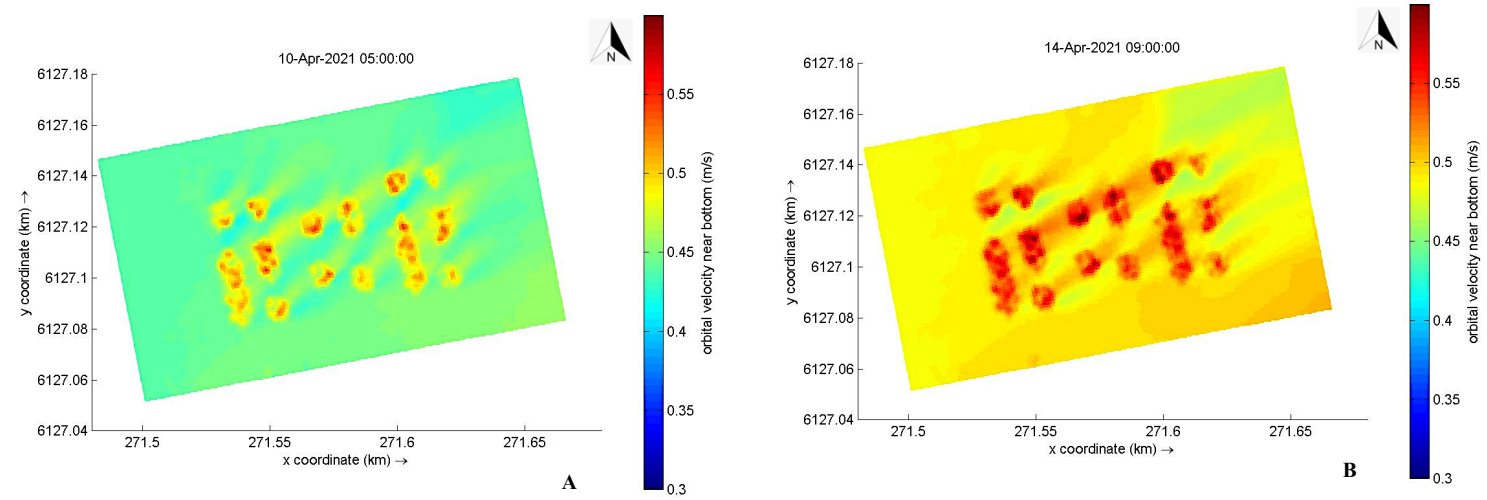

Fig 50: Orbital velocity near bottom trend with increased significant wave height. (A) the 10th of April 2021, at 5:00am; (B) the 14th of April 2021, at 9:00am. A decrement of the orbital velocity can be observed in the central part of the reef (light blue), while the magnitude of the orbital velocity increases at the reef's crests (red).

DISCUSSION

Oyster reefs construction and/or restoration projects have been developed in different countries (Piazza et al. 2005; Furlong 2012;) and some are relatively recent (Salvador de Paiva et al. 2018). Those that have been monitored (Piazza et al. 2005; Melancon et al. 2013) to examine their long-term effects have shown positive ecological and hydrodynamical results, particularly in preventing shoreline recession, and in some cases, they can be considered high-potential elements for self-sustained coastline protection (Chauvin 2016). The direct influence of submerged shellfish reefs, such as the Glenelg shellfish reef on hydrodynamics affecting the coastal environment is still poorly researched, while most research has examined the effects of fringing oyster reefs, coral reefs, and other coastal protection systems (e.g., breakwaters), through the use of numerical and experimental models, most of them performed in wave flumes (Neelamani and Rajendran 2002; Zidan, A.R. et al. 2012; Vijay et al. 2020).

In the current study, the use of Delft3D software for the analysis of hydrodynamics within the shellfish reef in the area of Glenelg (South Australia), identified how the submerged reef caused minimal wave energy dissipation, compared to other coastal environments such as fringing coral reefs, rocky platforms and living shorelines. The term living shorelines indicates those habitats that provide protection from erosion, such as salt marshes and oyster reefs in the intertidal zone (Gittman et al. 2016). Key parameters were investigated to evaluate the performance of living shorelines in Louisiana (USA), such as reef's crest height and water depth (Piazza et al. 2005; Morris et al. 2019). It was observed that with reef's crest only 5 centimetres below mean water level, the mean wave energy dissipation corresponded to the 42%, while with emerged crest (water level 1 centimetre below the crest), the mean wave energy dissipation increased to 83%. The obtained data (Piazza et al. 2005; Spiering et al. 2018; Morris et al. 2019) suggest how reducing the distance between the boulders 'crests and the water surface could potentially improve the wave energy attenuation capability of the Glenelg shellfish reef.

The amount of energy dissipated by the Glenelg shellfish reef with higher significant wave height, corresponding to 1.28 meters increased up to a 36% more (Figure 47) compared to low significant wave height conditions. The relationship between an increasing significant wave height and amount of dissipated energy was previously observed with the installation of artificial Reef Balls^{TM} in the Dominican Republic and Mexico (Harris 2004) and on submerged trapezoidal artificial reefs (Vijay et al. 2012), with wave dissipation increasing as significant wave height increased.

In a laboratory experiment with a trapezoidal submerged breakwater (Vijay et al. 2020), energy dissipation increased even with minor changes in significant wave height, from 0.1 meters to 0.4 meters. It is important to highlight the difference between the above-mentioned case studies and the current study; first of all, the difference in the depth of the Glenelg reef and the one of the submerged structures considered above; the Reef Balls^{TM} were placed at a depth ranging from 1.6 meters to 2.0 meters, in a microtidal environment (tidal range of 0.4 meters), with crests at 0.3-0.8 meters below the mean sea water level, while for the engineered

breakwater (Vijay et al 2020.) the wave flume where the experiment was performed was 1 meter deep, with the breakwater's crest located few centimetres below the mean water level. The area where the Glenelg reef is located is mesotidal, with a tidal range of > 2 meters and waves that can reach 2 meters during extreme weather events.

The current study also shows how the Glenelg reef has the capacity to reduce significant wave height by the 4% in the areas behind the reef's boulders towards the eastern side of the reef, during days of calm. On the contrary, on the crests of the reef's structures, the significant wave height increases by the 7.5% (Figure 41). During periods of storms, the decreasing in significant wave height resulted in 15% more (Figure 43), from the reef boulder's crests to the reef inner areas. If the reef was placed in shallower waters, closer to the shoreline, or if the boulders were taller, that could potentially lead to waves breaking on the reef and consequent wave energy dissipation; those results were confirmed by a laboratory study (Li et al. 2018) and by the natural shallow submerged breakwater at Narrowneck, Queensland (Turner 2006) (Figure 51). The Narrowneck Reef extends from 150 meters to 600 meters offshore and 350 meters alongshore, with the breakwater's crest at 1.5 meters deep at low tide (Jackson et al. 2007) and wave breaking about 200 meters from the coastline, when waves have a significant wave height around 1 meter.

Picture removed due to copyright restrictions.

Original available online:
https://www.swellnet.com/news/swellnet-dispatch/2017/11/07/narrowneck-artificial-reef-nears-completion-updated

Figure 51: Narrowneck reef, Queensland. *Source: SwellNet (2017)*

It must be pointed out how for the wave breaking to happen, not only the location of the submerged structure (deep or shallow) has to be considered, but also wave conditions. In fact, wave height increases when it starts to interact with the substrate (seafloor or structure), because of friction (Cialone and Smith 2007), usually where the water depth is half of the wavelength. In the analysed conditions, the combination of reef's boulders depth and relatively low significant wave heights (< 1.5 meters) prevent the wave breaking process to happen.

Potential improvement of the performance of the Glenelg shellfish reef on wave breaking, wave energy dissipation as a successful coastal management resource could be further enhanced with oyster growth. Oyster growth and colonization will cause the multiple reef's boulders to be higher and the reef's crests closer to the water surface. At this stage, data available for oyster growth at the Glenelg shellfish reef are not available, however for the first restoration project in South Australia, the Windara reef, a growth rate of about 0.5 mm

per month was seen, from an height of 9 mm from the boulders 'crests to the highest shell, in May 2018, to a 15 mm height in May 2019 (Reeves and Gillies 2019), a lower rate than the one recorded for the living shorelines in Louisiana (Piazza et al. 2005), which reached 1.5 mm per month. Although a difference in growth rate is present, the results for the Windara shellfish reef are encouraging, with an oyster density of 674 organisms per m^2 and a total of 6.1 million specimens on the reef and a similar trend is plausible for the Glenelg shellfish reef.

The growth and survival of the Glenelg shellfish reef, as well as its potential function of shoreline protection are strongly influenced by wave-driven currents and consequently, sediment dynamics. During the current study, a 22% reduction in orbital velocity was observed at the seafloor, on the central areas of the reef, during the storm events of the 10^{th} and 14^{th} of April 2021. It must be pointed out, how orbital velocities near the bottom had minimal values, ranging from 0.3 m/s to 0.5 m/s (Figure 50 (A) and (B)). Those results suggest a potential ability of the shellfish reef to reduce the velocity of wave-driven currents, resulting in shoreline stabilization and protection from erosion but for now, the effect of the reef is negligible. Although the role of the Glenelg shellfish reef on sediment dynamics was not addressed in the current study, a potential similar effect would be consistent with previously obtained results in the Netherlands (Borsje et al. 2011), where it was observed an attenuation of hydrodynamics and the accumulation of incoherent sediment along the shoreline, while in the United States, a decrease in shoreline retreat of almost 50% was detected (Piazza et al. 2005).

CONCLUSIONS

The current study highlights the following conclusions:

1) The Delft3D WAVE model correctly simulated the variation of the significant wave height, with good accuracy (85%). An overestimation of wave height was observed during the two storm periods, characterized by greater wave energy.

2) A decrease in bed shear stress was observed in the inner areas of the Glenelg reef, towards the Northwest. In contrast, an increasing bed shear stress was detected on the crests of the reef's boulders.

3) A minimal variation in significant wave height, corresponding to a 7.5% decrease, occurred from the crests of the reef's boulders to the central areas of the reef, during days lower wave energy events. The significant wave height decreased of the 15%, from the boulders ‘crests to the inner zones of the reefs, during higher wave energy events.

4) The results obtained for wave energy dissipation showed that most of the dissipation occurred on the crests of the reef's structures, compared to the inner zones of the reef. Furthermore, a 36% increase in dissipated energy, was observed during a storm event, when the significant wave height increased.

5) Orbital velocities near the bottom were characterized by minimum values, corresponding to a magnitude ranging between 0.3 m/s and 0.5 m/s, during events with greater wave energy and a 22% decrease, in the inner reef areas. Due to the severely low magnitude of water orbital velocities, it can be affirmed that the reef has no influence on the parameter.

The analysis of the obtained results with numerical modelling indicates that the Glenelg reef mildly influences the hydrodynamics of the area of interest, with a minimal increasing in wave energy dissipation, particularly during storm events.

Literature cited

Alleway, H. K., & Connell, S. D. (2015). Loss of an ecological baseline through the eradication of oyster reefs from coastal ecosystems and human memory. *Conservation Biology*, *29*(3), pp. 795-804.

Amante, C. J., & Eakins, B. W. (2016). Accuracy of interpolated bathymetry in digital elevation models. *Journal of Coastal Research*, *76*(10076), pp. 123-133.

Barras, J. A., Beville, S., Britsch, D., Hartley, S., Hawes, S., Johnston, J., ... & Suhayda, J. (2003). *Historical and projected coastal Louisiana land changes: 1978-2050*, p. 39. Louisiana, US: United States Geological Survey.

Beck M.W., Brumbaugh R.D., Airoldi L., Carranza A. et al. (2011) Oyster Reefs at Risk and Recommendations for Conservation, Restoration, and Management. *BioScience*, *61*, pp.107-116.

Black, J.A. (1986). Oceans and coasts, an introduction to oceanography. Wm. C. Brown Publishers. Dubuque, Iowa.

Black, K. (2001). Artificial surfing reefs for erosion control and amenity: theory and application. *Journal of Coastal Research 34*, pp. 1-14.

Borsje, B. W., van Wesenbeeck, B. K., Dekker, F., Paalvast, P., Bouma, T. J., van Katwijk, M. M., & de Vries, M. B. (2011). How ecological engineering can serve in coastal protection. *Ecological Engineering*, *37*(2), pp. 113-122.

Bourman, R. P., Murray-Wallace, C. V., & Harvey, N. (2016). *Coastal Landscapes of South Australia*. University of Adelaide Press.

Boyd, J. D. (2006). Evaluation of ADCP wave measurements. Naval Postgraduate School. Monterey, California.

Brown, E., Colling, A., Park, D., Philips, J., Rothery, D., Wright, J. (1999). Waves, tides, and shallow-water processes. The Open University, United Kingdom.

Bryars, S., Brook, J., Meakin, C., McSkimming, C., Eglinton, Y., Morcom, R., Wright, A. and Page, B. (2016). Baseline and predicted changes for the Upper Gulf St Vincent Marine Park, DEWNR Technical report 2016/24, Government of South Australia, through Department of Environment, Water and Natural Resources, Adelaide.

Bureau of Meteorology (2021). South Australian Tides Tables. Viewed 22nd October 2021. Available at http://www.bom.gov.au/oceanography/projects/ntc/sa_tide_tables.shtml

Bye, J. A. (1976). Physical oceanography of Gulf St. Vincent and Investigator Strait. *Natural history of the Adelaide region*, 143-160.

Carter, R. W. G. (2013). Coastal environments: an introduction to the physical, ecological, and cultural systems of coastlines. Elsevier.

Chauvin, J. M. (2018). Wave attenuation by constructed oyster reef breakwaters.

Cialone, M. A., & Smith, J. M. (2007, November). Wave transformation modelling with bottom friction applied to southeast Oahu Reefs. In *10th International workshop on Wave Hindcasting and Forecasting & Coastal Hazard Assessment*, pp. 1-12.

Colling, A. (2001). Ocean circulation (Vol. 3). Butterworth-Heinemann.

Crawford C., Edgar G., Gillies C.L., Heller-Wagner G. (2019) Relationship of biological communities to habitat structure on the largest remnant flat oyster reef (*Ostrea angasi*) in Australia. Marine and Freshwater Research.

Dame, R. F., & Patten, B. C. (1981). Analysis of energy flows in an intertidal oyster reef. *Marine Ecology Progress Series*, *5*(2), pp. 115-124.

Damiani, L., Bruno, M.F., Malcangio, D., Molfetta, M., Saponieri, A., Pratola, L., Mali, M. and Valentini, N. (2016). Correntometria e Onde di Marea. Corso di Regime e Protezione dei Litorali. Politecnico di Bari. Viewed 25th July 2021, available at https://docs.dicatechpoliba.it/filemanager/189/info%20corso%20A.A.%202016_2017/slides%20del%20corso/18_CORRENTOMETRIA%20E%20ONDE%20DI%20MAREA.pdf

Danovaro, R. (2013). Biologia marina: biodiversità e funzionamento degli ecosistemi marini. De Agostini Scuola.

D'Asaro, E. A., Eriksen, C. C., Levine, M. D., Niiler, P., & Van Meurs, P. (1995). Upper-ocean inertial currents forced by a strong storm. Part I: Data and comparisons with linear theory. *Journal of Physical Oceanography*, *25*(11), pp. 2909-2936.

Deltares (2016). OpenEarth. Viewed 25th September 2021, available at https://publicwiki.deltares.nl/display/OET/OpenEarth

Deltares (2018). RGFGRID. Generation and manipulation of structured and un-structured grids, suitable for Delft3D-FLOW, Delft3D-WAVE or D-Flow Flexible Mash. User Manual, version 5.00, 18 April 2018. Available at https://usermanual.wiki/Pdf/RGFGRIDUserManual.483699550/view

Deltares (2021). Delft3D-FLOW. Simulation of multi-dimenstional hydrodynamic flows and transport phenomena, including sediments. User Manual, version 3.15, 27 September 2021, available at https://content.oss.deltares.nl/delft3d/manuals/Delft3D-FLOW_User_Manual.pdf

Demirbilek, Z., Nwogu, O.G. and Ward, D.L. (2007). Laboratory study of wind effect on runup over fringing reefs, Report 1: data report.

de Paiva, J. N. S., Walles, B., Ysebaert, T., & Bouma, T. J. (2018). Understanding the conditionality of ecosystem services: The effect of tidal flat morphology and oyster reef characteristics on sediment stabilization by oyster reefs. *Ecological Engineering*, *112*, pp. 89-95.

Edyvane, K. S. (1999). Coastal and marine wetlands in Gulf St. Vincent, South Australia: understanding their loss and degradation. *Wetlands Ecology and Management*, *7*(1), pp. 83-104.

Ferrario, F., Beck, M., Storlazzi, C. et al. (2014). The effectiveness of coral reefs for coastal hazard risk reduction and adaptation. *Nature Communication 5*(3794), pp. 1-9.

Franklin, G., Mariño-Tapia, I. and Torres-Freyermuth, A. (2013). Effects of reef roughness on wave setup and surf zone currents. *Journal of Coastal Research*, 65(10065), pp. 2005-2010.

Gallop, S. L., Bosserelle, C., Eliot, I., & Pattiaratchi, C. B. (2012). The influence of limestone reefs on storm erosion and recovery of a perched beach. *Continental Shelf Research*, *47*, pp. 16-27.

Gallop, S.L., Bosserelle, C., Elliot, I., Pattiaratchi, C.B. (2013). The influence of coastal reefs on spatial variability in seasonal sand fluxes. *Marine Geology*, *344*, pp. 132-143.

Gilby B.L., Olds A.D., Henderson C.J., Ortodossi N.L., Connolly R.M., Schlacher T.A. (2019) Seascape context modifies how fish respond to restored oyster reef structures. *ICES Journal of Marine Science*, *76*, pp. 1131-1139.

Gillies C.L., McLeod I.M., Alleway H.K., Cook P. et al. (2018) Australian shellfish ecosystems: Past distribution, current status and future direction. *PLOS ONE 13* (1), pp. 900-914

Gillies C.L., Castine S.A., Alleway H.K., Crawford C. et al. (2020) Conservation status of the Oyster Reef Ecosystem of Southern and Eastern Australia. *Global Ecology and Conservation, 22*(e00988), pp. 1-16.

Gittman, R. K., Peterson, C. H., Currin, C. A., Joel Fodrie, F., Piehler, M. F., & Bruno, J. F. (2016). Living shorelines can enhance the nursery role of threatened estuarine habitats. *Ecological Applications*, *26*(1), 249-263.

Gutiérrez, J. L., Jones, C. G., Strayer, D. L., & Iribarne, O. O. (2003). Molluscs as ecosystem engineers: the role of shell production in aquatic habitats. *Oikos*, *101*(1), pp. 79-90.

Jackson, L. A., Corbett, B. B., McGrath, J. E., Tomlinson, R. B., & Stuart, G. (2007). Narrowneck Reef: review of seven years of monitoring. *Shore and Beach*, *75*(4), pp. 67-79.

Hardy, I., Huang, Z., Smith, D., & Fletcher, C. H. (2020). Numerical Modeling of Beach Morphological Change: A Case Study of Kaanapali Beach, Maui, Hawaii. *International Journal of Ocean and Coastal Engineering*, *3*(01n02), 2050002.

Harris, L. E. (2004). Submerged reef structures for beach erosion control. In *Coastal Structures 2003*, pp. 1155-1163.

Healy, T.R., 1980. Erosion and Sediment Drift on the Bay of Plenty coast. Soil and Water, August, pp. 12-14.

Housego, R.M. and Rosman, J.H., 2016. A model for understanding the effects of sediment dynamics on oyster reef development. *Estuaries and Coasts*, *39*(2), pp.495-509.

Komar, P. D. (1998). Wave erosion of a massive artificial coastal landslide. *Earth Surface Processes and Landforms: The Journal of the British Geomorphological Group*, *23*(5), pp. 415-428.

Knauss, J. A. (2005). III. Currents. *The Sea, Volume 2: the Composition of Sea-Water Comparative and Descriptive Oceanography*, *2*, (235).

Langley, R. B. (1998). The UTM grid system. *GPS world*, *9*(2), 46-50.

La Peyre, M., Furlong, J., Brown, L. A., Piazza, B. P., & Brown, K. (2014). Oyster reef restoration in the northern Gulf of Mexico: extent, methods, and outcomes. *Ocean & Coastal Management*, *89*, pp. 20-28.

Lesser, G. R., Roelvink, J. V., Van Kester, J. A. T. M., & Stelling, G. S. (2004). Development and validation of a three-dimensional morphological model. *Coastal engineering*, *51*(8-9), pp. 883-915.

Li, X., Zhang, W., & Wu, D. (2018). Assessment of Wave Energy Dissipation and Stability of Breakwater with Varied Geometries Subjected to Strong Waves. In *Earth and Space 2018: Engineering for Extreme Environments*, pp. 991-1003. Reston, VA: American Society of Civil Engineers.

Losada, I. J., Lara, J. L., Guanche, R., & Gonzalez-Ondina, J. M. (2008). Numerical analysis of wave overtopping of rubble mound breakwaters. *Coastal engineering*, *55*(1), pp. 47-62.

Lowe, R. J., Falter, J. L., Monismith, S. G., & Atkinson, M. J. (2009). A numerical study of circulation in a coastal reef-lagoon system. *Journal of Geophysical Research: Oceans*, *114*(C6), pp. 1-18.

Mann, K. H., & Lazier, J. R. (2013). Dynamics of marine ecosystems: biological-physical interactions in the oceans. John Wiley & Sons.

Masselink, G., & Puleo, J. A. (2006). Swash-zone morpho dynamics. *Continental Shelf Research*, *26*(5), pp. 661-680.

Masselink, G., & Hughes, M. G. (2014). An introduction to coastal processes and geomorphology. Routledge.

McAfee D., O'Connor W.A., Bishop M.J. (2017) Fast-growing oysters show reduced capacity to provide a thermal refuge to intertidal biodiversity at high temperatures. *Journal of Animal Ecology*, *86*, pp. 1352-1362

McClenachan, G. M., Donnelly, M. J., Shaffer, M. N., Sacks, P. E., & Walters, L. J. (2020). Does size matter? Quantifying the cumulative impact of small-scale living shoreline and oyster reef restoration projects on shoreline erosion. *Restoration Ecology*, *28*(6), pp. 1365-1371.

Melancon, E.J. Jr., Curole, G.P., Ledet, A.M., and Fontenot, Q.C. (2013). Operations, Maintenance, and Monitoring Report for Terrebonne Bay Shore Protection Demonstration (TE-45). Coastal Protection and Restoration Authority of Louisiana, Thibodaux, Louisiana.

Morris, R. L., Bilkovic, D. M., Boswell, M. K., Bushek, D., Cebrian, J., Goff, J., ... & Swearer, S. E. (2019). The application of oyster reefs in shoreline protection: Are we over-engineering for an ecosystem engineer? *Journal of Applied Ecology*, *56*(7), pp. 1703-1711.

Muste, M., Yu, K., Pratt, T. C., & Abraham, D. (2002). ADCP measurements at fixed river locations. In *Hydraulic Measurements and Experimental Methods,* pp. 1-12.

National Ocean Service (NOAA) (2021). Tidal Currents 1. National Oceanic and Atmospheric Administration. U.S. Department of Commerce. Viewed 7th September 2021. Available at https://oceanservice.noaa.gov/education/tutorial_currents/02tidal1.html

Narayan, S., Beck, M. W., Reguero, B. G., Losada, I. J., Van Wesenbeeck, B., Pontee, N., ... & Burks-Copes, K. A. (2016). The effectiveness, costs and coastal protection benefits of natural and nature-based defences. *PloS one*, *11*(5), e0154735.

Neelamani, S., & Rajendran, R. (2002). Wave interaction with T-type breakwaters. *Ocean Engineering*, *29*(2), pp. 151-175.

Ocean Illumination (2020). Ocean Contour Acoustic Doppler Data Processing. Software Users Guide.

Piazza, B. P., Banks, P. D., & La Peyre, M. K. (2005). The potential for created oyster shell reefs as a sustainable shoreline protection strategy in Louisiana. *Restoration Ecology*, *13*(3), pp. 499-506.

Pickrill, R. A., & Mitchell, J. S. (1979). Ocean wave characteristics around New Zealand. *New Zealand journal of marine and freshwater research*, *13*(4), pp. 501-520.

Piper, J.D.A. (1978). Geological and geophysical evidence relating to continental growth and dynamics and the hydrosphere in Precambrian times: a review and analysis. *Tidal Friction and the Earth's Rotation*, pp. 197-241.

Poate, T., Masselink, G., Austin, M., Dickson, M. and Kench, P., 2016. Observation of wave transformation on macro-tidal rocky platforms. *Journal of Coastal Research*, (75 (10075)), pp. 602-606.

Powers, S. P., Peterson, C. H., Grabowski, J. H., & Lenihan, H. S. (2009). Success of constructed oyster reefs in no-harvest sanctuaries: implications for restoration. *Marine Ecology Progress Series*, *389*, pp. 159-170.

Quataert, E., Storlazzi, C., Van Rooijen, A., Cheriton, O., & Van Dongeren, A. (2015). The influence of coral reefs and climate change on wave-driven flooding of tropical coastlines. *Geophysical Research Letters*, *42*(15), pp. 6407-6415.

Ranasinghe, R., & Turner, I. L. (2006). Shoreline response to submerged structures: A review. *Coastal Engineering*, *53*(1), pp. 65-79.

Reeves, S., Nedosyko, A. and Gillies, C. (2019). The Nature Conservancy Windara Reef Technical Report 2019. The Nature Conservancy Australia. Viewed 1st November 2021. Available at https://www.researchgate.net/publication/343640156_The_Nature_Conservancy_Windara_Reef_Technical_Report_2019

Reguero, B. G., Losada, I. J., & Méndez, F. J. (2019). A recent increase in global wave power as a consequence of oceanic warming. *Nature communications*, *10*(1), pp. 1-14.

Schulte, D. M., Burke, R. P., & Lipcius, R. N. (2009). Unprecedented restoration of a native oyster metapopulation. *Science*, *325*(5944), pp. 1124-1128.

Scyphers, S. B., Powers, S. P., Heck Jr, K. L., & Byron, D. (2011). Oyster reefs as natural breakwaters mitigate shoreline loss and facilitate fisheries. *PloS one*, *6*(8), e22396.

Songnian, J. (1992). ADCP Observation and Its Data Processing Technique [J]. *Ocean Technology*, *1*.

Southwell M., Veenstra J., Adams C., Scarlett E., Payne K. (2017) Changes in sediment characteristics upon oyster reef restoration, NE Florida, USA. *Journal of Coastal Zone Management 20* (442).

Spiering, D. W., Kibler, K. M., Kitsikoudis, V., Donnelly, M. J., & Walters, L. J. (2021). Detecting hydrodynamic changes after living shoreline restoration and through an extreme event using a Before-After-Control-Impact experiment. *Ecological Engineering*, *169*, 106306.

Stride, A. H. (1982). Tidal currents of the continental shelf. In *Offshore tidal sands*, Springer, Dordrecht, pp. 10-26.

Sumich, J. L., & Pinkard-Meier, D. R. (2016). Introduction to the biology of marine life. Jones & Bartlett Learning.

Talley, L. D., Pickard, G.L., Emery, W.J. and Swift, J.H. (2011). Descriptive physical oceanography: an introduction. Academic press.

Telesca, L., Belluscio, A., Criscoli, A., Ardizzone, G., Apostolaki, E. T., Fraschetti, S., ... & Salomidi, M. (2015). Seagrass meadows (*Posidonia oceanica*) distribution and trajectories of change. *Scientific reports*, *5*(1), pp. 1-14.

The Nature Conservancy (2019). Restoring Adelaide's lost shellfish reefs: more fish and cleaner water for South Australians to enjoy. Shellfish reef restoration Project Management Plan. The Nature Conservancy and Government of South Australia 2019.

The Nature Conservancy (2020). Restoring Adelaide's lost shellfish reefs: returning Australia's endangered marine habitat to Adelaide's shore. https://www.natureaustralia.org.au/what-we-do/our-priorities/oceans/ocean-stories/adelaide-oyster-reef/, viewed February 2021.

The Nature Conservancy and the Department for Environment and Water (2019). Community input to inform the final location of an Adelaide metropolitan shellfish reef. Consultation Report prepared by The Nature Conservancy and the Department for Environment and Water. Adelaide, South Australia.

Turner, I. L. (2006). Discriminating modes of shoreline response to offshore-detached structures. *Journal of waterway, port, coastal, and ocean engineering*, *132*(3), pp. 180-191.

Van Leeuwen, B., Augustijn, D. C., Van Wesenbeeck, B. K., Hulscher, S. J., & De Vries, M. B. (2010). Modelling the influence of a young mussel bed on fine sediment dynamics on an intertidal flat in the Wadden Sea. *Ecological Engineering*, *36*(2), pp. 145-153.

Vijay, K. G., Neelamani, S., Nishad, C. S., & Sahoo, T. (2021). Gravity wave interaction with multiple submerged artificial reefs. *Proceedings of the Institution of Mechanical Engineers, Part M: Journal of Engineering for the Maritime Environment*, *235*(2), pp. 607-622.

Villanoy, C., David, L., Cabrera, O., Atrigenio, M., Siringan, F., Aliño, P., & Villaluz, M. (2012). Coral reef ecosystems protect shore from high-energy waves under climate change scenarios. *Climatic change*, *112*(2), pp. 493-505.

Walles, B., Troost, K., van den Ende, D., Nieuwhof, S., Smaal, A. C., & Ysebaert, T. (2016). From artificial structures to self-sustaining oyster reefs. *Journal of Sea Research*, *108*, pp. 1-9.

Wanis, P., & Hull, M. (2011). New technology impacts on ADCP instruments. In *OCEANS'11 MTS/IEEE KONA*, IEEE, pp. 1-5.

Weppe, S., Healy, T., Scarfe, B., & Immenga, D. (2009). Shoreline response to an offshore submerged multifunction reef at Mount Maunganui, New Zealand. *Coasts and Ports 2009: In a Dynamic Environment*, 648.

Wiberg, P.L., Taube, S.R., Ferguson, A.E. et al. (2019). Wave Attenuation by Oyster Reefs in Shallow Coastal Bays. *Estuaries and Coasts*, *42***,** pp. 331–347.

Woodroffe, C.D. (2002) Coasts: form, processes, and evolution. Cambridge University Press.

Yamashita, T., Yoshioka, H., Kato, S., Ming, L., & Shimoda, C. (1999). ADCP observation of nearshore current structure in the surf zone. In *Coastal Engineering,* pp. 787-800.

Zidan, A. R., Rageh, O. S., Sarhan, T., & Esmail, M. (2012). Effect of breakwaters on wave energy dissipation (Case study: Ras El-bar Beach, Egypt). *Int Water Technol J*, *2*(4), pp. 268-283.